Resistive Heating for Self-healing Materials Based on Ionomeric Polymers

by

Matt Castellucci

Thesis submitted to the Faculty of the
Virginia Polytechnic Institute and State University
in partial fulfillment of the requirements for the degree of

Master of Science

in

Mechanical Engineering

Dr. Donald J. Leo, Chair
Dr. Daniel J. Inman
Dr. Scott W. Case
Dr. Vishnu Baba Sundaresan

June 24, 2009
Blacksburg, Virginia

Keywords: self-healing, damage detection

Resistive Heating for Self-healing Materials Based on Ionomeric Polymers

Matt Castellucci
Virginia Polytechnic Institute and State University, 2009
Advisor: Donald J. Leo, Ph.D.

Abstract

Self-healing materials have received considerable development in the last decade. Recent results have demonstrated healing in polymeric materials via a chemical reaction using a healing agent or response to thermal treatment. The goal of this research is to develop a new composite material, for application in wire insulation, that can detect damage and heal itself using resistance heating. The composite material is composed of a conductive network embedded in a polymer matrix. The conductive network is used for damage detection and resistive heating. A matrix material is used that melts when heated and flows to fill damage. External electronic circuitry is used to implement a damage detection algorithm and apply current for resistive heating. Surlyn 8940 is chosen as the polymer matrix and carbon fibers are selected for the resistive heating elements. Methods for melt processing Surlyn are developed and used to produce Surlyn films and composite samples where carbon fiber is embedded in a Surlyn matrix. A finite element model of the resistive heating process is developed to predict the temperature distribution.

Thermal imaging is used to characterize resistive heating while optical microscopy and tensile testing are used to characterize healing. Damage detection using capacitive measurements is demonstrated and characterized. The self-healing composite is placed on top of another conductive material such as in the wire insulation application. Capacitance measurements are made using the conductive network inside the composite is used as one electrode and the wide conductor as the second electrode.

Acknowledgments

First I would like to thank my research advisor, Dr. Donald J. Leo, for the opportunity to be a part of this work. I would also like to thank Dr. Dan Inman and Dr. Scott Case for their support as members of my advisory committee. NextGen Aeronautics has made this research possible and I would like to thank them for doing so.

I would like to thank my fellow graduate students at the Center for Intelligent Material Systems and Structures at Virginia Tech, specifically Steve Anton, Andy Duncan, and Andy Sarles for their assistance and advice throughout my time at CIMSS. I would like to thank Vicki Long and Matt Hunley for their kind assistance with running experiments.

Finally, I would like to extend a very sincere thank you to Dr. Vishnu Baba Sundaresan for his direction and assistance throughout my time as a graduate student. Working with Vishnu has been a great experience and I am always grateful.

MATT CASTELLUCCI

Contents

List of Tables

List of Figures

Nomenclature

WHR	Width heal ratio
w_b	Crack width before healing
w_a	Crack width after healing
C	Capacitance
R	Resistance
I	Current
A	Amps
V	Volts
W	Watts
J	Joules
Q	Heat energy
P	Power
T	Temperature
t	Time
ρ	Density
c_p	Specific heat
k	Thermal conductivity
h	Heat transfer coefficient
Ra_L	Rayleigh number
Nu_L	Nusselt number
g	Acceleration due to gravity
β	Thermal expansion coefficient
ν	Kinematic viscosity

α	Thermal diffusivity
L	Length
σ	Electrical conductivity

CHAPTER 1

INTRODUCTION

Damage detection and healing are unique properties of biological systems. In such systems a damage event triggers internal processes that generate the healing response. Examples include the clotting of blood, healing of a broken bone, and repair of damaged organ tissue. To imitate this unique property in nature engineers have drawn inspiration from biological materials and processes to develop autonomous self-healing materials.

Traditional engineering materials require human attention to identify and repair damage. In most cases a routine inspection program or preventative maintenence results in identification of the damage; without this maintenance the damage goes undetected until failure occurs. When damage is detected in traditional materials it requires human intervention to replace or repair a part of the system and cannot be healed or repaired without human action. Engineering materials that can autonomously detect and heal damage have the potential to reduce costs by reducing the amount of human interaction with a given system, minimize system downtime, and reduce the need for part replacement. In some applications, such as deep space probes, human interaction in the form of inspection/repair is not possible and the ability to autonomously heal damage might significantly reduce the chance of failure. The limitation and inability of traditional engineering materials to heal themselves due to a damage and the necessity for designing a self-healing material suitable for mission critical applications forms the motivation for this thesis. The work presented in this document was a part of the developmental effort by Virginia Tech to develop a self-healing wire insulation material for aerospace applications.

In some self-healing materials healing is autonomically triggered by the damage event. Other self-healing materials require external damage detection methods, using an electronic circuit to trigger healing. To date, research in the area of self healing materials has generally involved polymers or polymer composites (Trask and Bond (2007), Wu et al.

(2008)), with several different approaches towards autonomic healing. In this chapter an overview of self-healing materials and damage detection will be discussed as it relates to this work.

1.1 Self-healing Concepts and Materials

The recent advances in material science, micro/nanoscience, and polymer chemistry have resulted in various methods to heal a damage. Different forms of interaction, namely chemical, thermal, electrical, and optical, between novel materials and composite materials have been proposed for self-healing. Chemical reactions restore strength to damaged material by hardening a liquid healing agent that has been delivered to the damage site. Heating the material using electrical resistance heating, magnetic induction heating, and ballistic penetration (puncture of a thin film by a small pellet fired from an air gun) are other methods demonstrated to heal damage in some materials. Many self-healing materials developed to date are limited to one healing event in a particular location but some are capable of healing multiple (successive) damages in the same location. Reviews of recent developments in self-healing materials are presented by Wu et al. (2008), N. Sottos (2007), and Trask and Bond (2007).

The first research in the area of self healing materials involved hollow fibers filled with a liquid healing agent and embedded in a polymer matrix. In these materials damage to the composite would rupture the hollow fibers, releasing the healing agent to fill the damage site and heal the damage. Fig. 1.1 shows the configuration of self healing materials based on embedded microcapsules or hollow fibers.

Early examples of self healing materials include Dry and Sottos (1993) and White et al. (2001). In Dry and Sottos (1993) hollow glass fibers filled with a chemical were embedded in a polymer matrix. Upon cracking of the hollow fiber, caused by mechanical loading, the chemical stored in the hollow fiber is released into the crack to heal the composite. A finite amount of damage is required in order to rupture the hollow fiber, release healing agent, and repair the material. The chemical contained inside the hollow fibers is usually an adhesive or air-curing polymer/monomers. Healing using this teqhnique was demonstrated in both impact and fiber pull-out testing. Similar to hollow fiber based self-healing, microcapsules filled with healing agent embedded in the polymer matrix have been used for

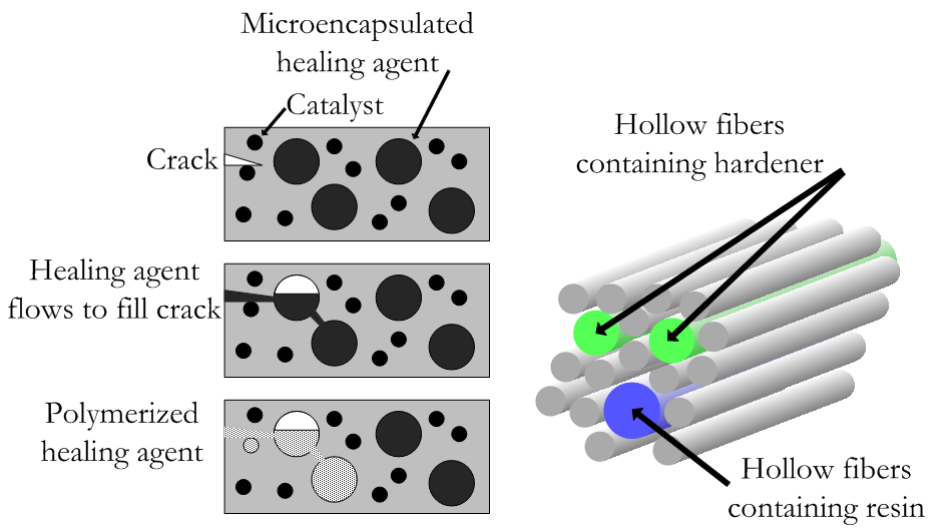

(a) Microcapsules.

(b) Hollow fibers.

Figure 1.1: Healing materials based on microencapsulation (a) generally have catalyst dispersed in the matrix and healing agent contained within embedded microcapsules. Damage to the material causes microcapsules to rupture, allowing healing agent to flow into the damage. Catalyst dispersed in the matrix causes the healing agent to polymerize, healing the damage. Healing materials based on hollow fibers (b) work employ a similar strategy but with healing fluids contained within hollow fibers instead of microcapsules.

designing a self-healing material. Upon crack intrusion the microcapsules rupture allowing healing agent to flow into the crack. An embedded catalyst triggers polymerization of the healing agent with up to 75% fracture toughness recovery reported (White et al. (2001)). Trask and Bond (2006) investigated the flow of healing resin from the hollow fiber into the damage and performed optical microscopy on damaged and undamaged laminates with hollow fibers Williams et al. (2007a).

R. S Trask and Bond (2007) investigated the effect of hollow glass fibers on bulk laminate mechanical properties and healing efficiency, using both glass and carbon fiber reinforced polymer composites in flexural bend testing. A fixed load was applied in the bending test to initiate damage. Inclusion of hollow fibers resulted in an initial flexural strength reduction of 16% as compared to a laminate without hollow fibers, but healing was able to recover 87% of undamaged strength. Quasi-static impact testing of carbon fiber reinforced polymer resulted in 97% recovery in flexural strength, where maximum reduction in undamaged flexural strength was 8%. Addition of the hollow fibers resulted in an initial strength reduction but gave the benefit of greater damage tolerance.

Initial investigations of hollow fiber based self healing materials have used two-part healing agents. In these materials one hollow fiber contains resin and an adjacent hollow fiber contains hardener. In order to heal the damage both fibers must break allowing both resin and hardener to flow into the damage. Single part adhesives have demonstrated healing capability but with lower strength recovery (Wang (2007)).

Privman et al. (2007) reported initial progress with a continuum rate equation method to model fatigue in composites reinforced with nanoporous glue-carrying fibers. Computational modeling of self-healing materials is still in its infancy (Balazs (2007)).

Similar to embedded hollow fibers, vascular networks have been used for self-healing materials. In this approach a network of interconnected hollow fibers carry a pressurized healing fluid that is designed to release during damage, flow into the damage, and heal it. Networks may be either 'tree' or 'grid' type. Toohey et al. (2007) demonstrated the capability to heal multiple damage events in the same locality using a microvascular network. Bejan et al. (2006) investigated different 'grid' network configurations with differing channel diameters to determine the most efficient delivery method. The embedded network has negligible effect on the mechanical properties of the material and demonstrated complete recovery with epoxy resin as the healing agent (Williams et al. (2007b)). Williams and

Bond (2007) determined the critical failure modes of a vascular network system and compared results to the human circulatory system. This work represents the first consideration of failure modes of vascular network self healing materials. Optimal configurations of the vascular network system were developed by Williams and Bond (2008) and Aragn et al. (2008). In their work, Williams and Bond (2008) present a biomimetic analysis and derive an expression for optimal vessel diameter that agrees with constructal theory. In their work the effects of deviation from optimal vessel diameter are also considered. Aragn et al. (2008) used a multi-objective genetic algorithm approach to design vascular networks with constraints such as network efficiency, redundancy, and void volume fraction.

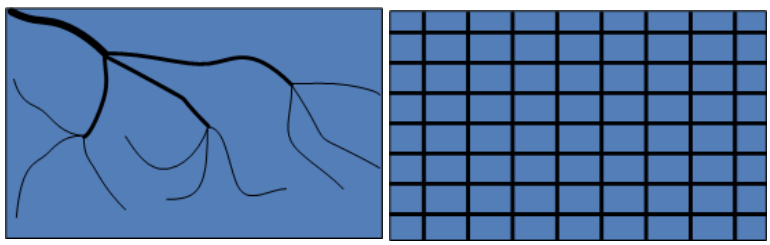

(a) Tree arrangement. (b) Grid arrangement.

Figure 1.2: Vascular networks may be arranged as a 'tree' (a) or 'grid' (b) configuration within the material.

The majority of work in the area of self healing materials to date has involved embedded microcapsules, and good healing results have been reported. Typical materials are microencapsulated dicyclopentadiene reacting with Grubb's catalyst embedded in the polymer matrix to heal damage (White et al. (2001)). Brown and White (2002) investigated the effects of size and concentration of microcapsules on fracture toughness and healing efficiency; they reported as much as 90% recovery of fracture toughness after healing. A similar method is used in Kessler et al. (2003) to demonstrate up to 80% recovery in carbon fiber reinforcement at elevated temperatures, with up to 45% recovery at room temperature. Yin et al. (2007) reported 111% recovery in fracture toughness in epoxy, with no loss of fracture toughness compared to neat epoxy. In Brown et al. (2005) the fatigue life was extended up to 218% using the healing material. A fatigue life extension of 30 times that of a similar, non-healing, polymer was reported in Jones and White (2007) by adding wax microspheres and quickly dissolving catalyst to previous microsphere-based materials.

When reinforced with glass fabric the healing efficiency in the epoxy material improved to 68%. Keller (2007) reported 70-100% recovery of tear strength using microencapsulated resin and microencapsulated crosslinker added to Polydimethylsiloxane (PDMS) matrix.

While microcapsule size has typically been about 180μm, an in situ encapsulation technique capable of reducing capsule diameter to 220nm with wall thickness 77nm was recently published by (Blaiszik et al. (2008)). Rule et al. (2007) developed a method to choose microcapsule size and concentration based on predetermined crack size.

In addition to chemical reactions, thermal treatments have also been used to demonstrate healing. Kalista (2003) demonstrated healing in ionomeric materials following a ballistic puncture. In this work several ionomeric films, including DuPont Surlyn 8940, were punctured by a small pellet. Ionomer films autonomically healed following the damage event. It was concluded that heat generated by the puncture caused the ionomer to locally melt and heal the damage and that the penetration site recovered to an air-tight condition (Kalista (2003)). Other damage modes were also evaluated for their ability to demonstrate healing. Sawing and projectile puncture generated enough heat in Surlyn to cause healing but puncture by nail did not (Kalista and Ward (2007) and Kalista (2003)). It can be concluded that a high rate of energy input is required to melt Surlyn at the damage site to heal the damage. Varley and van der Zwaag (2008a) extended these results that simulated ballistic impact by rapidly pulling a rod through the polymer material. In their subsequent work Varley and van der Zwaag (2008b) studied the fundamental processes through which the ionomer Surlyn 8940 is able to autonomically heal ballistic damage. Examination of impact surfaces by scanning electron microscope (SEM) indicated that an elastic response accounts for the initial rebounding while a viscous response provides for final healing. It was also demonstrated in this work that healing arose from the ionic clusters in the ionomer and that the clusters are a critical component to ballistic healing.

Others have demonstrated the ability to use heat to heal damage in Surlyn through different heating mechanisms. Owen (2006) embedded several types of magnetic particles in Surlyn 8940 and used induction heating to heal crack-type damage. Samples with α-Fe_2O_3, γ-Fe_2O_3, and Ni-Zn Ferrite (3, 6, and 10% by volume) were prepared. Samples were heated with 1.5-10kW, 50kHz to 13.56MHz induction heating units. Heating/healing was achieved with all samples but the heating response was faster and higher temperature achieved with higher concentration of magnetic particles. (Healing was evaluated by

examination under optical microscope (10X) and through tensile testing.)

Other polymeric materials in which the covalent bonds can be reformed have been used to demonstrate self-healing. Chen et al. (2002) developed a polymeric material that can re-form the covalent bonds in the polymer when heated. In this material 30% of intermonomer linkages disconnect on heating the sample above 120°C and then re-connect upon cooling. This process can be used to heal successive damages in the same location. Williams (2007) propose an electrically conductive polymer as a 'stimulus-responsive' material. When a microcrack forms the number of electron pathways would decrease causing electrical resistance to increase. Electrical circuitry connected to the material could monitor and detect the change in resistance and trigger the application of an electric field. The microcrack is the source of increased resistance; therefore the applied electric field should generate heat locally at the damage (Williams (2007)). In this work healing was achieved with an external heat source and the theory of higher resistance at the damage site leading to localized heat generation was not tested.

Generating heat to heal damage may be achieved through electrical resistive heating. One potential problem with this approach is inadvertently generating heat away from the locality of damage, for example due to high contact resistance. Kwok and Hahn (2007) investigated the use of carbon fibers as heating elements for self-healing composites. In this work carbon fiber composite samples were prepared and the relative resistance of several different contact types tested. Resistive heating was demonstrated and compared to finite element simulation results. In their results, contact resistance was dominant over short distances while composite resistance dominated over long distances. Contact resistance was reduced by removing the resin-rich top layer and using large area contact electrodes.

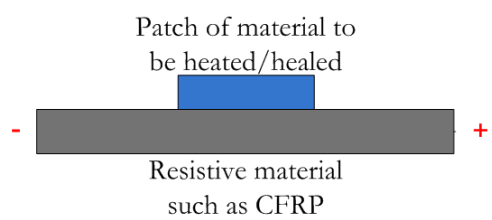

Figure 1.3: Resistive heating for healing has been demonstrated by placing a patch of material to be heated/healed on top of a resistive material such as carbon fiber reinforced polymer (CFRP). Passing current through the CFRP causes it to heat, transferring heat to the patch of healing material on top.

Park et al. (2008) used carbon fibers to generate heat due to electrical resistance and heal damage. In this work, mendomer, a polymeric material that heals when heated near the glass transition temperature, was applied to and cured on top of a carbon fiber/epoxy laminate. Current passed through carbon fibers generates heat in the laminate which transfers to the mendomer material on top of the laminate. The weakest bonds in the polymer chain are formed in the thermally reversible Diels-Alder dicyclopentadiene adduct; it is these bonds that break under loading. The material can be healed by heating close to the glass transition temperature where the broken chain ends recombine Park et al. (2008)). Damage was initiated using either a three-point bending fixture in an Instron load frame or by using a razor blade to scratch the surface. Electrical resistance heating of the carbon fiber/epoxy laminate successfully healed damage due to three-point bending in the mendomer patch. Damage due to razor blade scratch did not heal because the crack faces were not in physical contact when heated.

1.2 Damage Detection and Autonomous Self-healing

The science of detecting the presence of a damage in a material is referred to as damage detection or structural health monitoring (SHM). The self-healing material developed in this work is a wire insulation material and is not a structural application. Hence the term damage detection, instead of structural health monitoring, will be used to describe the work in this thesis. A distinction is made between damage detection and strain measurement. While strain measurement can be used to detect damage in a material, a certain level of strain may exist below which the material is not damaged but returns to its initial state when load is relaxed.

Many methods have been developed to monitor damage in structures such as beams, plates, bridges, and other large civil structures. Vibration-based methods and fiber optic sensors have been demonstrated for damage detection. Salawu (1997) prepared a review of literature related to using changes in natural frequency to detect structural damage. Reviews of vibration-based methods used to detect damage in a structure are presented in (Doebling et al. (1996), Doebling et al. (1998)). Modal parameters, such as frequencies, mode shapes, and modal damping, are dependent on properties of the structure such as mass, damping, and stiffness. Changes in the physical properties, due to damage, will

cause detectable changes in modal properties and hence modal measurements become valuable in detecting damage. Fiber optic sensors embedded in composite structures have been used to detect and locate damage as described in a review by Zhou and Sim (2002). Montalvao and Ribeiro (2006) present a review of similar techniques applied to composite structures. Other structural health monitoring methods have been developed based on non-destructive evaluations (NDE) such as acoustic (Dickinson and Fletcher (2009)), optical (Davila et al. (2009)), ultrasonic (Gupta et al. (2008)), and piezoelectric (Park et al. (2006)) measurements.

The previously described methods have been developed for mechanical and/or civil structures. The following is a review of damage detection technologies relevant to non-structural applications. Several authors have demonstrated damage detection by measuring changes in electrical resistance; more specifically, changes in resistance of embedded carbon fibers. Most reported work is in the area of carbon fiber reinforced polymer (CFRP) composites, but the same techniques apply when carbon fibers are embedded in any insulating material. Wen and Chung (2007) were able to detect irreversible damage in carbon fiber reinforced cement by measuring change in electrical resistance. Strain in the elastic region led to a resistance change of 1-7% while irreversible strain caused a change of 10-30%. The change in resistance is attributed to fracture of fibers at the damage site. Abry et al. (1999) measured strong changes in resistance as unidirectional CFRP laminates were loaded in flexure, sufficient to detect very low damage levels. Angelidis and Irving (2007) demonstrated damage detection in CFRP by measuring changes in electrical potential due to impact events. Results of the electrical potential measurements correlated well with damage measurements by c-scan.

Other electrical measurements have been used to detect damage. Martin (2004) used an impedance based method to detect damage in a composite plate. Tiefenbach et al. (2000) used impedance spectroscopy to detect microstructural damage in tetragonal zirconia polycrystals (TZP). Cracks were detected as changes in capacitive and resistive parts of the electrical impedance. Carlson et al. (2006) developed a flexible self-healing skin incorporating an array of LC circuits which are used to detect damage. Each LC circuit has a unique (undamaged) resonant frequency which is changed by damage. Monitoring circuitry is used to detect and locate damage. If the circuit elements could be embedded in a thin polymer film such methods will become relevant for self-healing wire insulation.

1.3 Modeling

Most of the work to date in the area of self healing materials has been experimental. Lee et al. (2004) used micromechanics simulations to evaluate composite properties and monte carlo simulation to model healing in polymers with embedded nanoparticles. Later, Balazs (2007) presents a review of recent developments in the area of computational studies related to self-healing systems. Topics discussed center around modeling nanoparticle flow into the damage site using techniques such as monte carlo and molecular dynamics simulations. Barbero et al. (2005) developed a continuum mechanics model that includes healing. Privman et al. (2007) developed a continuum rate equation model for healing composites reinforced with glue-carrying nanoporous glass fibers.

The finite element method has also been applied to simulate healing in materials. Burton et al. (2006) used the finite element method to model crack closure using shape memory alloy (SMA) wires. Upon heating the damaged composite pre-strained SMA wires undergo a martensitic phase transformation causing the crack to close, thus healing. Maiti et al. (2006) present a numerical model, a combination of fatigue crack propagation and a contact algorithm for crack closure, for analysis of microcapsule-based self healing materials.

Kwok and Hahn (2007) used finite element analysis to model resistive heating behavior of carbon fibers embedded in polymer matrix. Park et al. (2008) performed finite element analysis on a carbon fiber in epoxy composite for resistive heating of a patch of healing material applied on top of the composite laminate.

1.4 Motivation

While the development of self-healing materials has many industrial applications, the research conducted for this thesis was in direct support of developing a self-healing material for use in wire insulation. Damage to wire insulation can be difficult or impossible to locate by manual inspection and failure of the insulation is often catastrophic in nature. Since insulation damage is difficult or impossible to locate visually an electronic means of detecting damage is very desirable. The research in this thesis covers the development of a new self-healing material with damage detection capability for use in a wire insulation application.

1.5 Outline of Work

The work conducted for this thesis led to the following contributions to the area of self-healing materials and damage detection:

- Development of a new self-healing composite material based on carbon fibers embedded in Surlyn. Unique characterization techniques, such as crack width measurement and thermal imaging, were used in the characterization of this material.
- Development of a new method for detecting damage based on monitoring change in capacitance measurements.

The following items highlight the objectives of research work conducted for this thesis:

- Develop and use melt processing methods to prepare composite samples of carbon fibers embedded in a Surlyn matrix. Samples will be prepared in several configurations for testing the healing and damage detection capabilities of the material.
- Characterize the resistive heating capabilities of the material. Determine what electrical power and time duration are required to effectively heal damage in samples.
- Develop a method to detect damage in the wire insulation using electronic measurements. Characterize the relationship between the extent of damage and change in a measured parameter.
- Model resistive heating and heat conduction within the material and predict temperature distribution in the polymer as a function of time.

CHAPTER 2

SAMPLE FABRICATION AND CHARACTERIZATION

The self-healing material developed in this work uses resistive heating in carbon fiber to melt ionomeric Surlyn matrix to repair a damage in the material. This chapter discusses the architecture of the composite to design and fabricate the material, characterize heating in Surlyn for an applied electrical current, demonstrate healing of a simulated damage and quantify the healing process using a new metric for non-structural applications. The methods presented in this chapter, while yielding samples of controlled geometrical and electrical properties, are not suited for mass production. With this in mind, mass production methods for fabricating the composite material are proposed.

Optical microscopy and tensile test techniques used to characterize healed samples are discussed. Results of healing tests are presented and demonstrate that this method can completely heal surface damages given sufficient electrical power input and careful design of carbon fiber heating elements in Surlyn.

2.1 Self-healing Polymer Composite

The self-healing material presented in this thesis is a composite material prepared by embedding carbon fibers in Surlyn 8940 (referred to as 'Surlyn' from this point forward). Surlyn is a commercially available sodium ionomer manufactured by DuPont and is used in various applications including golf ball covers. The thermoplastic Surlyn is an ethlene/methacrylic acid (E/MAA) copolymer with the MAA groups partially neutralized with sodium ions. Surlyn has melt temperature 95°C and is chosen for its low mass and previously demonstrated healing capabilities (Kalista (2003), Owen (2006), Kalista and

Ward (2007), Varley and van der Zwaag (2008a), and Varley and van der Zwaag (2008b)). Carbon fibers are selected as heating elements for the Surlyn based self-healing composite due to their low electrical resistance and resistive heating potential. Other properties, such as low mass and high strength, make this an attractive option over other heating elements such as nickel chromium wire. The carbon fiber used in this work is obtained from Aerospace Composite Products (except the material used for the resistive heating/healing demonstration sample, which is produced using carbon fiber originating from an unkown source). Carbon fiber purchased from Aerospace Composite Products are fabrics woven from bundles having 1000 individual carbon fibers per bundle. These bundles, referred to as 1k bundles in this thesis, provide a known and consistent amount of carbon fibers that can be used as the fundamental carbon fiber unit for hand fabrication of the composite. The number of 1k bundles will be varied to obtain uniform heating throughout the Surlyn/carbon fiber composite.

There are many possible arrangements of carbon fiber bundles in Surlyn. Typical (structural) composite materials are manufactured using either woven fabric, made from bundles ranging from one thousand to many thousands of individual reinforcing fibers, or unidirectional reinforcement. The composite may be made from many layers of woven fabric or unidirectional reinforcement stacked in different angular orientations. Many methods exist for embedding reinforcement in the matrix material.

For the initial resistive heating/healing demonstration sample a bundle of about 12k carbon fibers is distributed in a unidirectional fashion between two layers of 200μm thick Surlyn films. Carbon fiber bundles are exposed on the two ends of the composite and serve as electrodes for the resistive heating/healing test. Initial formal resistive heating/healing test samples follow a similar configuration. In samples designed for both damage detection and resistive heating the carbon fiber bundles are arranged as a network of parallel resistors inside Surlyn. Copper wire electrodes embedded in the composite connect the fiber bundles to external circuitry. Flat plate type samples are used to demonstrate the damage detection and resistive heating/healing technology.

The arrangement of carbon fiber bundles as a network of parallel resistors facilitates damage detection using both resistive and capacitive methods and also allows resistive heating. Low power resistive heating for healing is made possible by providing a low-resistance conductive path. Copper wire electrodes/carbon fiber bundles are used to con-

nect the parallel network to external circuits. By varying the length and number of 1k carbon fiber bundles that make up the parallel network the resistance of the sample can be tuned to provide a low value. Resistances of 5-10Ω provided good heating with low power input of less than 10W. In order to achieve sample resistances of 5-10Ω six 1k bundles of carbon fibers are used and the copper electrodes are spaced about 20mm apart. Even though electrode spacing, number of fibers, and number of fiber bundles is controlled the success rate of sample preparation is only about 30%, that is, about 30% of samples produced had resistance of 5-10Ω. The remaining samples had higher resistances, up to about 60Ω, which would not work for resistive heating because current draw at the pre-set voltage is too low to provide sufficient heating. It is suspected that the higher resistances are caused by Surlyn getting in between carbon fiber bundles and copper electrodes during final processing. Larger samples are prepared for purposes of demonstrating damage detection and healing. These samples are similar to the parallel network samples; in fact they are composed of three parallel network samples prepared side-by-side inside one Surlyn film. The parallel networks in these samples are composed of five bundles of carbon fibers with copper electrodes. These samples are deliberately prepared with slightly different spacing between the copper electrodes in order to demonstrate that the damage detection and healing circuitry functions properly with differing resistances on each channel. Fig. 2.1 shows the initial resistive heating/healing demonstration sample, the parallel network sample for damage detection and healing, and the three element film. Many other configurations of carbon fiber bundles in Surlyn are possible.

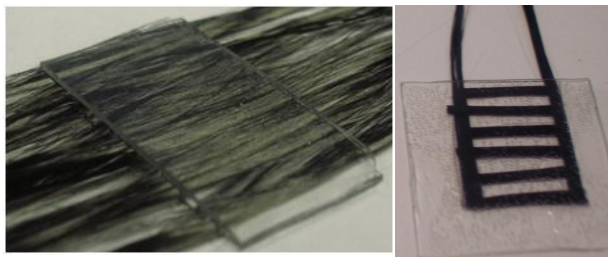

(a) (b)

Figure 2.1: Carbon fibers embedded in Surlyn for the initial resistive heating demonstration (a), carbon fiber bundles as network of parallel resistors inside Surlyn (b).

2.2 Self-Healing Wire Insulation

The new composite material is developed primarily as a healing layer for wire insulation. Current wire insulation in the target application is a three-layer composite of polytetrafluoroethylene (PTFE or teflon) and polyimide (kapton), arranged teflon-kapton-teflon (TKT). The healing layer is designed to integrate with the existing TKT insulation, being placed within the TKT composite. The multilayer wire insulation is composed of three or four thin film layers as shown in Fig. 2.2. These configurations are based on the addition of the healing layer (Surlyn/carbon fiber layer) to existing wire insulation configurations developed for specific application requirements. Existing wire insulation in the current application is typically a three layer, PTFE-polyimide-PTFE insulation. The three layer configuration is polyimide-Surlyn/carbon fiber-PTFE (with polyimide in contact with the conductor). The four layer configuration is PTFE-polyimide-Surlyn/carbon fiber-PTFE.

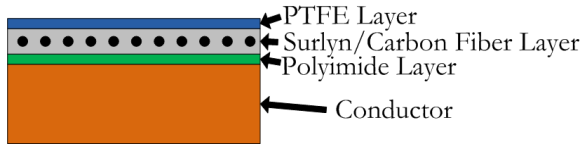

(a) Three layer insulation configuration.

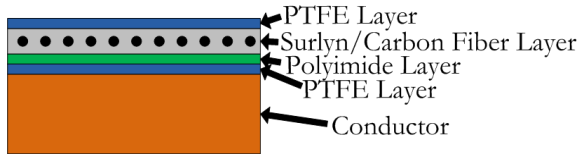

(b) Four layer insulation configuration.

Figure 2.2: Multilayer wire insulation layers. Conductor-polyimide-Surlyn/carbon fiber-PTFE (a) and conductor-PTFE-polyimide-Surlyn/carbon fiber-PTFE (b).

2.3 Fabrication of Test Samples

Surlyn is obtained in the form of pellets about 1mm in diameter. Films of varying thicknesses (150μm, 200μm, and 400μm) are produced by compressing Surlyn pellets in a melt press at 160°C and 3.5MPa using polyimide release films and steel borders to control film thickness. In some cases the initial pressing, when working directly with pellets, resulted

in films with air pockets. In such cases these films are cut into pieces and melt pressed again to eliminate air pockets. Films are compressed in the melt press for about 30sec; increasing press time does not significantly alter the film thickness or improve clarity of the films. Small composite films containing woven carbon fiber fabric are successfully prepared using the melt press.

Surlyn/carbon fiber films are prepared using a hot plate because pressure of the melt press causes carbon fiber bundles to flow with Surlyn and distort the fibers out of the desired position. Polyimide (kapton) release films prevented Surlyn from sticking to the hot plate or compression masses; Surlyn gets very sticky when heated above 160°C. Samples are prepared by arranging carbon fibers on one Surlyn film and then placing a second Surlyn film on top. The three-layer assembly (Surlyn-carbon fiber-Surlyn) is hand pressed into one film by placing the assembly on the hot plate and heating at 160°C for up to 5 minutes.

2.4 Healing Characterization

2.4.1 Healing Demonstration

The first step in characterizing healing in the composite was to demonstrate heating via resistive heating. The sample shown in Fig. 2.1 is fabricated with an arbitrary number of carbon fibers evenly dispersed in Surlyn for this demonstration. Electrical resistance of the embedded carbon fiber in this sample is measured to be 6Ω. A surface level damage is simulated in the sample by scoring it with a razor blade in such a way that the carbon fibers were not cut. A current of 0.5A is passed through the carbon fibers by applying a potential of 3V for a duration of 10min. Healing is qualitatively demonstrated in this sample by flexing the sample and observing the region near the crack before and after the application of electric field. Locking pliers are used so that the distance between the jaws is approximately equal when bending the sample before and after the experiment. Photographs of the sample before and after the experiment are shown in Fig. 2.3. It is observed that the application of electric potential heats the sample and closes the crack. Due to this observed effect, the application of an electric field across the ends of the carbon fibers in Surlyn is considered healing of the damage.

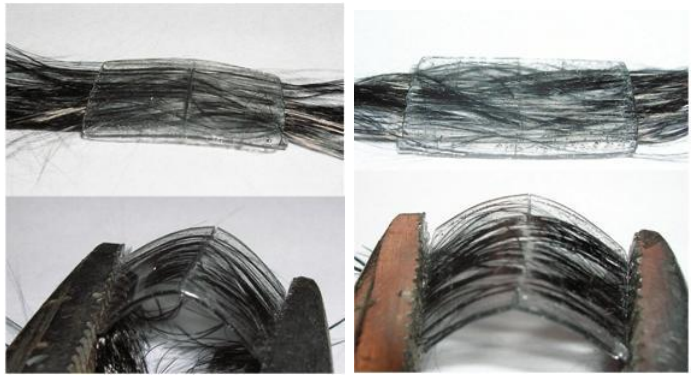

(a) (b)

Figure 2.3: Concept demonstration sample before (a) and after (b) resistive heating/healing. When flexed, crack remains closed in center region of sample after healing, as shown in (b) lower figure. This sample measures 10mm x 20mm.

2.4.2 Resistive Heating Characterization

Resistive heating of the sample for an applied electrical field is characterized through IR bolometry. The IR bolometric images of the resistive heating process leads to better understanding of heat transfer in Surlyn and temperature distribution for different carbon fiber arrangements affect healing. Infrared thermal images are recorded using a Fluke Ti25 thermal imaging camera on a sample with unidirectional carbon fiber bundles embedded in Surlyn. A photograph of the sample is shown in Fig. 2.4. The sample resistance is 3.5Ω. Resistive heating experiments are carried out at 2V (1.2W), 3V (2.6W), and 5V (7.2W). Images were captured at 15 second intervals starting before applying current (t = 0) and ending at 60 seconds. Fig. 2.5 shows the thermal imaging experimental setup and thermal images from the resistive heating experiments are shown in Fig. 2.6.

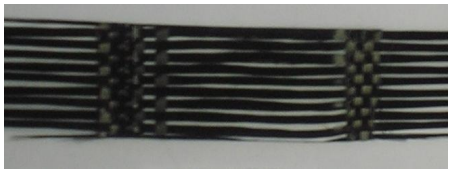

Figure 2.4: Sample used in resistive heating tests for thermal imaging.

Two very important observations are derived from the results of these experiments.

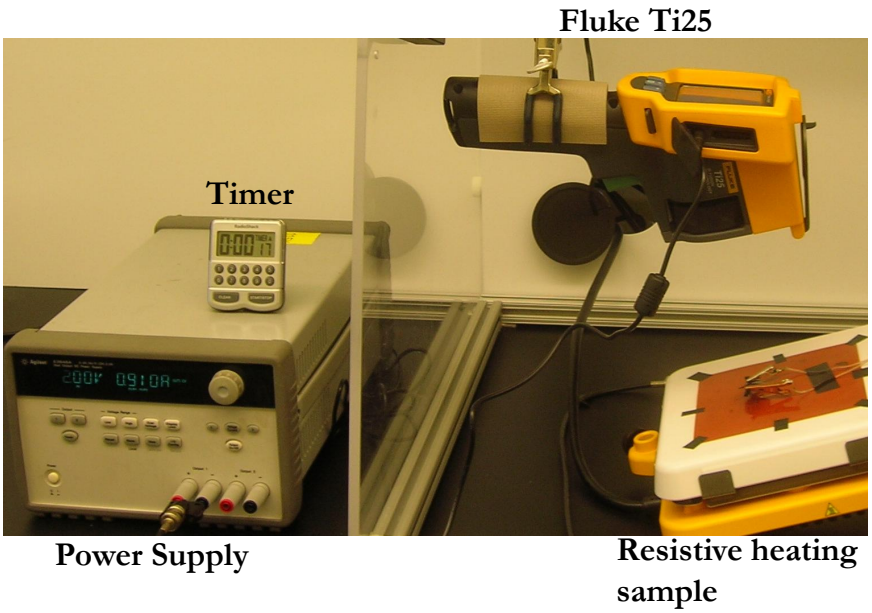

Figure 2.5: Thermal imaging experiment.

First, when higher power is applied more heat is generated in the sample and higher temperatures are achieved. Second, each experiment follows a definite trend of approaching a steady state temperature distribution. As heat generation due to joule heating balances heat transfer out of the sample, the sample approaches steady state temperature distribution.

Healing characterization testing is carried out based on these observations. When power applied is insufficient to heat the sample enough to heal damage, a higher power will heat the sample to a higher temperature. In each test there is a duration at which the sample is considered to have reached a steady state temperature distribution; continuing the experiment will not raise the temperature of the sample. Based on this observation healing characterization will be performed on the sample of identical geometry for the aforementioned power inputs and time duration.

2.4.3 Width Heal Ratio Characterization

Successful demonstration of the resistive heating/healing concept, experiments were conducted to characterize healing and quantify the healing process using a quantifiable damage metric. A jig is devised to create a damage of controlled dimensions in the sample and

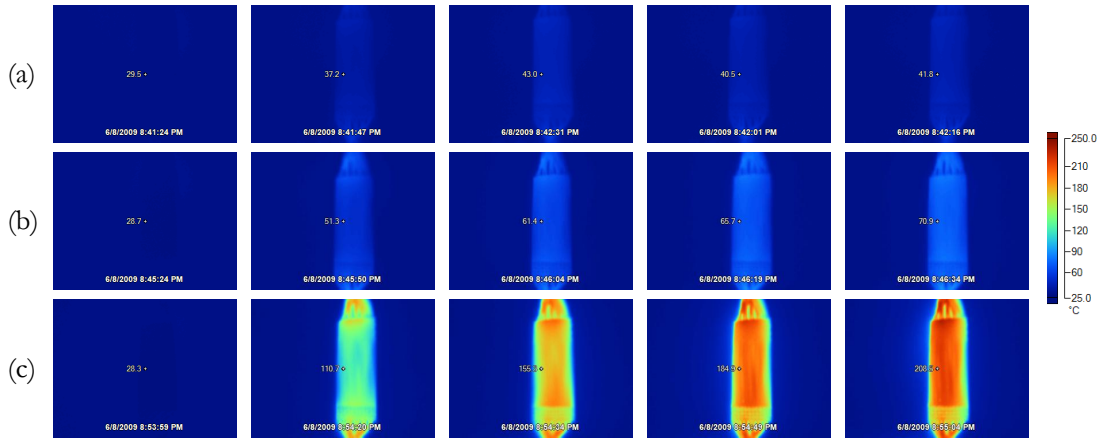

Figure 2.6: Thermal image results of resistive heating experiment. The sample is heated at 1.2W (a), 2.6W (b), and 7.2W (c). Test duration increases from t = 0 at left to t = 60sec at right, in 15sec intervals.

in a repeatable manner. A photograph of the jig is shown in Fig. 2.7. The jig consists of a razor blade mounted to a linear slide with a fixed mass attached. The fixed mass applies constant force to the razor blade which is advanced across the sample by the linear slide.

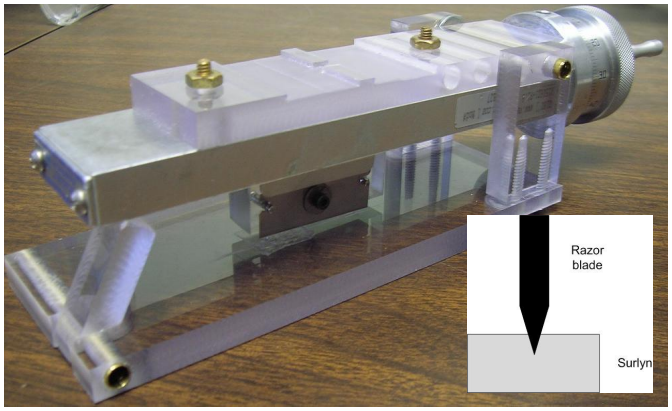

Figure 2.7: Jig used to damage samples in a controlled way. Inset shows geometry of razor blade used to damage Surlyn. Crack width is linerarly proportional to crack depth because only the triangular portion of the razor blade is used to damage Surlyn.

Damage is quantified by measuring the crack width under an optical microscope at 400X magnification. The width of the damage is measured at 5 locations along the damage and averaged to report the average width before healing (w_b). Due to the geometry of the razor blade used to damage the samples, crack width is linearly proportional to crack depth as shown in Fig. 2.7. The sample is heated by the application of an electrical field

at the ends of the carbon fiber for a finite duration. The sample is allowed to cool on removing the electrical field and the crack width is measured. This measured value after healing (w_a) is compared to the crack width before healing to calculate width heal ratio (WHR) as shown in Eq. (2.1). In healing results width heal ratio is typically reported as a percentage. Tensile tests are carried out in order to verify that crack closure restores strength to the Surlyn matrix.

$$WHR = \frac{w_b - w_a}{w_b} \tag{2.1}$$

where (w_b) is the crack width before healing, (w_a) is the crack width after healing, and WHR is the width heal ratio.

Composite samples are prepared for quantitative resistive heating/healing testing with the intent of studying the effect of varying crack widths and energy input on WHR. Samples are composed of Surlyn films measuring 10x20mm with one 12k bundle of carbon fibers embedded and evenly dispersed. Composite sample thickness averaged 0.75mm; carbon fiber content within the sample is estimated at 5% by mass. Average resistance of the samples is measured to be 1.87Ω. 200g and 1000g masses placed on the constant mass jig resulted in average crack widths of 14.4 and 28.3μm as measured under 400x optical microscope.

The objective of this test was to vary the amount of energy applied during the experiment. Different energy inputs are achieved by changing the time duration of the healing test while applying constant power. Resistive heating/healing was achieved by applying 1V for durations of 2min, 5min, and 10min. Energy input corresponding to the different durations averages 75, 185, or 370J while power input is a constant 0.62W. After healing crack widths were once again measured under 400x optical microscope and WHR calculated.

Samples demonstrated increased healing as input energy (test duration) increased. In tests with duration 2min almost no healing is observed. As duration increased to 5min and 10min increased healing is observed with approximately 50-60% healing achieved at 10min duration. Fig. 2.8 shows the results of this test, with each data point computed by averaging the WHR result from five samples.

Test results from the previous study demonstrate that energy input has a strong effect

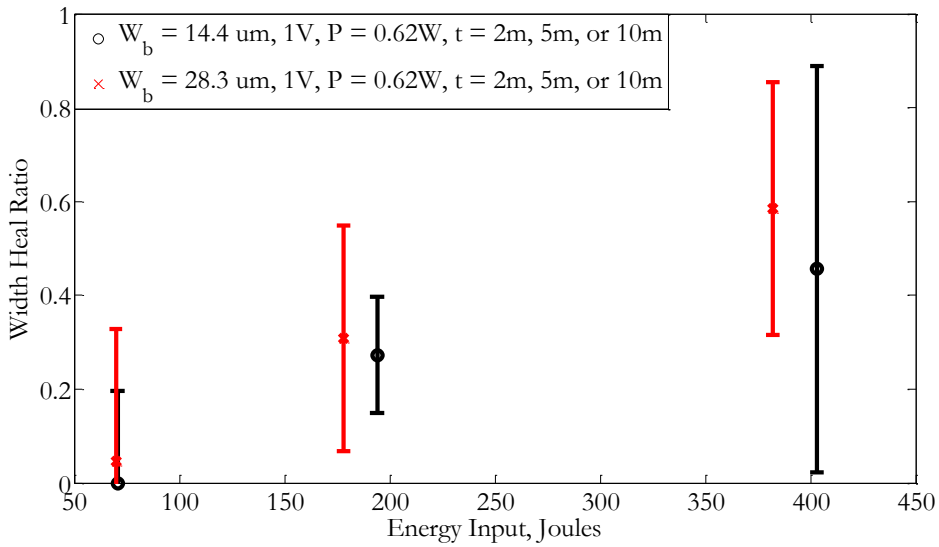

Figure 2.8: Healing results show that WHR increases as energy input increases. Increasing crack width has a smaller effect on WHR.

on WHR. Another set of samples, similar in geometry, is prepared to evaluate the effect of power input on healing. Average resistance in these samples is 1.7Ω. Damage is initiated with the constant mass jig using the 1000g mass; the resulting average crack width is 26.6μm. This amount of damage is very similar to the amount of damage (28.3μm average crack width) of samples from the previous study damaged using the 1000g mass.

Electrical power applied to the samples is increased to 2.5W by increasing the voltage to 2V. In order to make the results comparable to the previous tests, durations are chosen so that energy input would be nearly equal. Durations of 30sec and 90sec correspond to average energy inputs of 75 and 225J, respectively. These energy inputs compare well with those from the previous results: 75 and 185J. When power is increased to 2.5W much better healing is achieved. Over 80% healing is observed when test duration is 30s (energy 75J); when power is 0.62W and energy is 75J less than 10% WHR is observed. With 2.5W and duration 90sec (energy 225J) up to 100% healing is observed; when power is 0.62W and energy is 185J and average WHR is about 30%. Results of healing tests at 2.5W are shown in Fig. 2.9.

Two important conclusions may be drawn from this healing characterization experiment. First, healing is more dependent on power applied than energy applied. In tests with input energy of about 75J almost no healing is observed when applied energy is

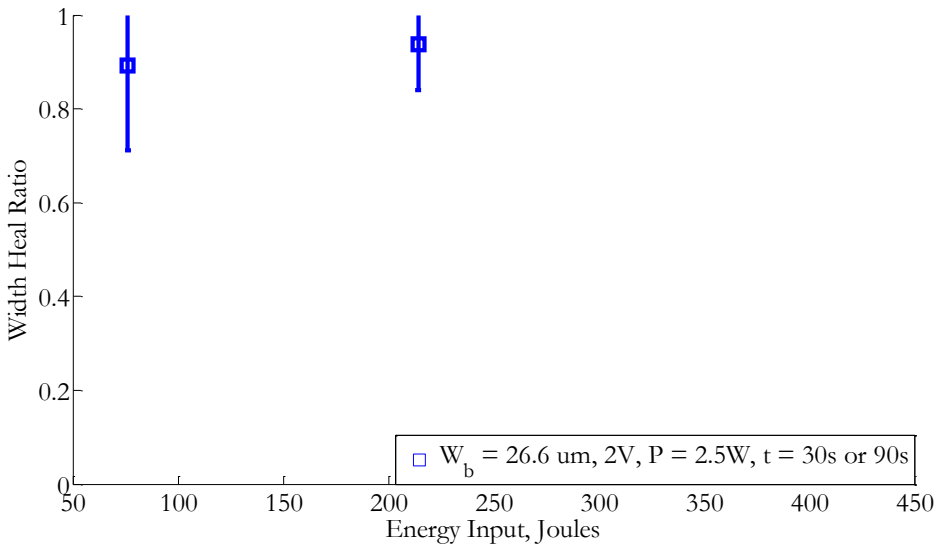

Figure 2.9: Healing results show that WHR is much higher when power is increased to 2.5W.

0.62W; when applied energy is 2.5W over 80% healing is observed. When applied energy averaged about 200J about 30% healing is observed when applied power is 0.62W; when applied power is 2.5W healing is over 85% and 100% in some cases. Secondly, given proper distribution of carbon fibers within Surlyn and sufficient power applied it is possible to heal damage. In some cases complete healing is observed in the sample. Distribution of fibers is observed to have an effect on healing as shown in Fig. 2.10; Surlyn has low thermal conductivity so areas further from heating fibers take longer to reach melt temperature.

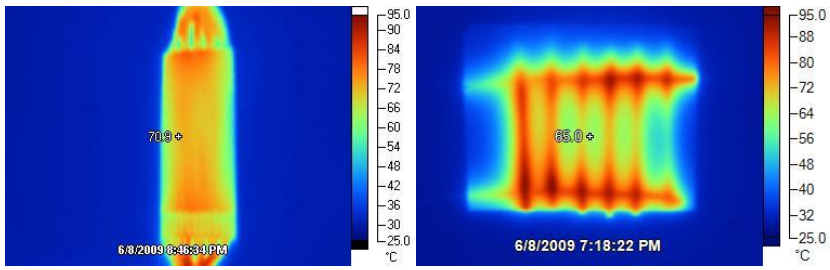

Figure 2.10: Distribution of carbon fiber heating elements affects temperature distribution in the composite. Uniform fiber distribution (left) and parallel network arrangement (right).

A very useful sample geometry consists of carbon fiber bundles arranged as a network of parallel resistors inside Surlyn, as shown in Fig. 2.1. This sample configuration facilitates healing and damage detection using both resistive and capacitive measurements. Samples

were prepared to evaluate the healing characteristics of this sample configuration with the goal of investigating different crack widths and healing test durations while holding power constant. Samples were produced with average resistance 8.66Ω using a parallel network of six 1k bundles of carbon fibers. Fig. 2.11 shows the distribution of sample resistance.

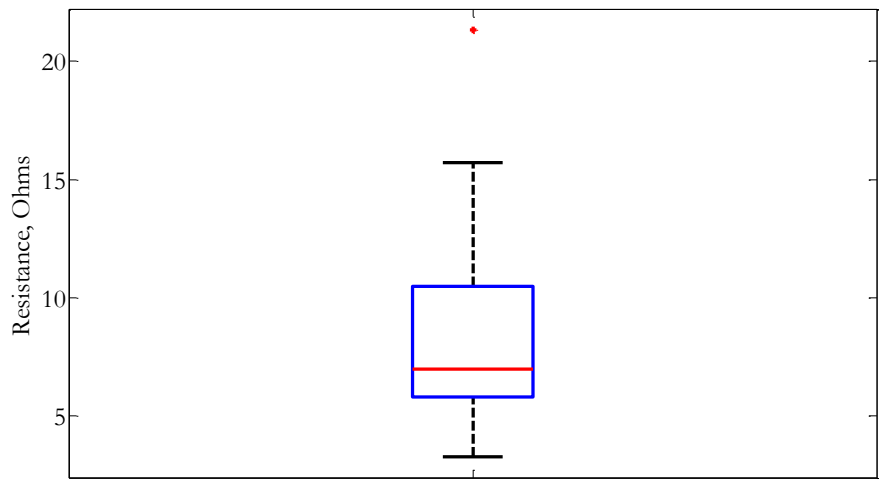

Figure 2.11: Distribution of sample resistances. Mean is 8.66Ω, standard deviation is 4.39Ω.

Thickness of the samples averaged 0.72mm with standard deviation 0.08mm. Samples were damaged using the fixed mass jig with masses 200g, 300g, and 500g. Attempts to damage sample using greater than 500g resulted in destroying sample by severing the carbon fiber bundles. Average crack widths were 61.8μm, 69.6μm, and 96.4μm using the 200g, 300g, and 500g masses, respectively. Healing tests were conducted by applying a constant 4V to the sample for 15, 30, 45, or 60 seconds. Due to variation in sample resistance current draw for a fixed voltage, power consumed and heat generated varied considerably. Fig. 2.12 shows the results of this testing. While variation in sample resistance was higher than intended, expected trends are evident from the results. First, healing has been demonstrated with this arrangement of carbon fiber inside Surlyn. Lower healing ratios with these samples, as compared to the results of Fig. 2.8 and Fig. 2.9, may be attributed to sample configuration. Samples healed for Fig. 2.12 have distinct bundles of carbon fiber dispersed in Surlyn, with a finite gap between fiber bundles. Heat transfer from the carbon fiber bundles to regions of Surlyn between fiber bundles is slow, potentially reducing healing ratio. Samples healed for Fig. 2.8 and Fig. 2.9 had an approximately

uniform distribution of carbon fiber thus reducing the heat transfer requirements.

As healing duration increases healing ratio increases, as expected. Generally, smaller crack widths resulted in higher heal ratios when duration was constant. For samples damaged using 200g and 300g masses there is some overlap in the heal ratios, due in part to a small difference in average crack widths (61.8μm when using 200g, 69.6μm when using 300g) before healing.

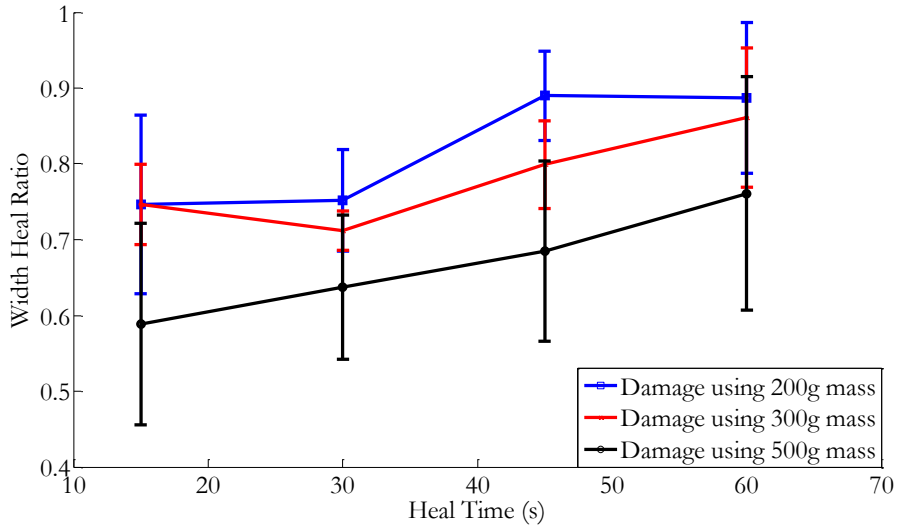

Figure 2.12: Results of healing tests with network of parallel resistors samples.

2.4.4 Tensile Testing

Tensile testing was used to evaluate the effectiveness of width heal ratio as a healing metric. Surlyn films were melt pressed at 160°C and 7MPa to thickness 0.15mm and trimmed to final size 40mm X 25mm. Pure Surlyn films were used, without embedded carbon fibers, for several reasons. Sample preparation is more controlled when carbon fibers are not embedded because fibers can shift position when the sample is pressed in the melt press. Carbon fibers are much stiffer (in tension) than Surlyn so fiber orientation would have a strong effect on tensile strength of the composite; fibers that shift during pressing would introduce variation in strength of the samples. Due to the high fiber stiffness, relative to the stiffness of Surlyn, a crack that does not damage any fibers may not affect the tensile strength of the composite, depending on fiber orientation. Lastly, damage to the carbon fibers cannot be healed; any healing that takes place is healing of Surlyn.

Surlyn films were damaged using the constant mass jig to an average crack width of 30.6μm with standard deviation 4.4μm as measured under 400x optical magnification. Samples were healed on a hot plate at 160°C for 90sec, after which the crack width averaged 1.5μm with standard deviation 1.3μm. Width heal ratio was 95.1%.

Tensile tests were conducted with extension rate 25mm/min with gage length 15mm. For undamaged samples the mode of failure was large plastic deformation; damaged samples showed slight plastic deformation followed by fracture at the damage. Healed samples also showed large plastic deformation. Fig. 2.13 shows the tensile test results.

Undamaged Surlyn failed (onset of plastic deformation) at 125.6N and 5.6mm extension; healed Surlyn failed (onset of plastic deformation) at 116.3N and 5.0mm extension. Strain energy is used to quantify the amount of damage imparted to the Surlyn film and amount of recovery after healing. Damaged Surlyn had 4.24% of the strain energy of undamaged Surlyn. Healed Surlyn films recovered 149.7% of strain energy as compared to undamaged films. These results confirm that when the damage closes, as determined by optical microscopy measurement based WHR of 95.1%, strength of the Surlyn material is restored.

2.5 Mass Production

All samples produced for this thesis are prototype samples hand fabricated one at a time. Large scale production of samples with controlled physical properties could benefit from more sophisticated manufacturing processes. For example, carbon fiber bundle placement and spacing between fiber bundles could be made more accurate using automated equipment. While melt pressing produced good quality films of uniform and predictable thickness, size is limited to about 100mm X 100mm. Attempts to produce larger films, close to the melt press platen size of 250mm x 250mm, resulted in films of very poor quality with high volume percentage of trapped air. Films produced by a larger melt press or sheet rolling process could produce high quality film in larger quantities. An automated process used to place carbon fiber bundles on the Surlyn films could improve the uniformity of bundle spacing (thus improving heating characteristics) and repeatability between samples.

Perhaps the area in greatest need of a mass production process is for self-healing wire

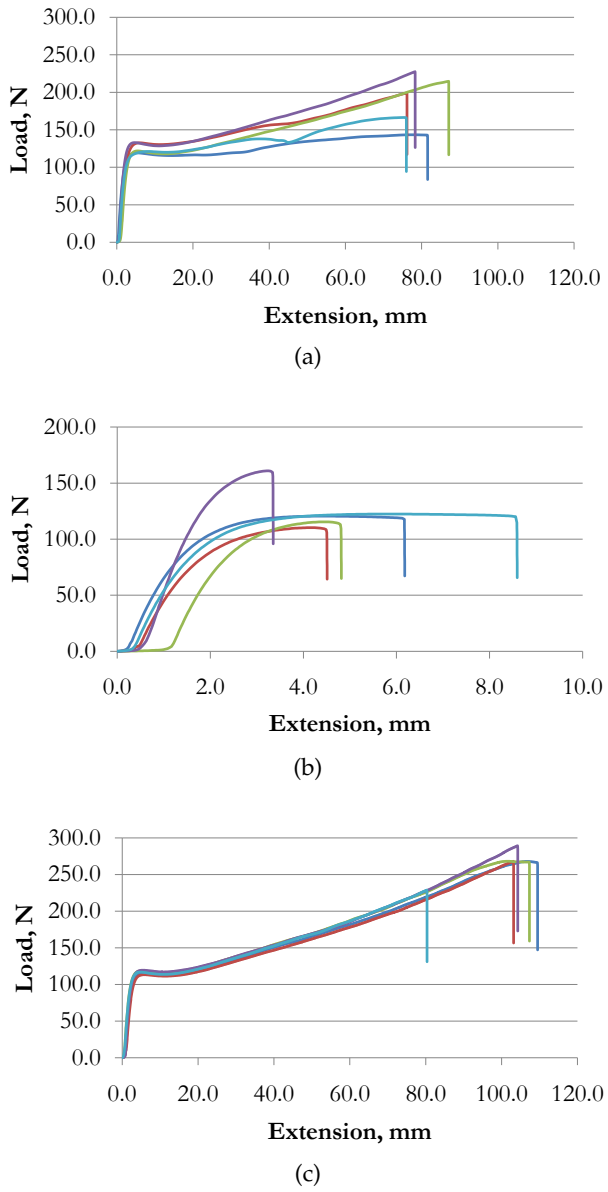

Figure 2.13: Tensile test results. For damaged Surlyn (b) samples fractured at less than 10mm extension, while undamaged (a) and healed (c) Surlyn samples had extensions over 80mm.

insulation samples. Current state-of-the-art extruding and winding processes can be modified to manufacture carbon fiber based self-healing wire insulation layers. In this work multilayer wire insulation components were hand wrapped around copper wires of varying diameter. Producing a composite film suitable for wrapping around a wire was difficult; thinner films were prepared that conformed to the wire better. Carbon fibers were arranged in a unidirectional fashion within Surlyn for these films for processing simplicity. The best samples were produced with large diameter copper wires and very thin composite films. After all insulation components were wrapped onto the wire a heat gun was used to soften the Surlyn in the healing layer so that a more permanent insulation was formed. While several prototype wire insulation samples were made they do not represent realistic wire insulation or contain parallel networks of carbon fibers as developed for damage detection.

2.6 Chapter Summary

Resistive heating/healing has been demonstrated both qualitatively, by observing crack closure under controlled bending, and quantitatively by crack width measurements. In some cases complete healing was demonstrated. Resistive heating/healing is more dependent on power supplied than energy; lower power/longer duration tests were less successful at healing than higher power/shorter duration tests. Temperature distribution is dependant on the arrangement of carbon fiber heating elements within the sample. Tensile tests have confirmed that healing quantified by crack width measurements restores strength of the material.

CHAPTER 3

DAMAGE DETECTION AND AUTONOMOUS SELF-HEALING

The healing characterization experiments discussed in the previous chapter demonstrated complete recovery from a surface crack. The amount of time required to heal a damage was found to be dependent on the input power. It was also established that a minimum power is required to produce any healing in the material. The self-healing concept developed in this work requires outside intervention to initiate healing in the material and hence must be combined with a damage detection technique. Current damage detection technology has focused on structures or structural materials. The current techniques available for damage detection in wire insulation material are not suitable for real-time monitoring.

In this chapter a damage detection technique based on monitoring change in capacitance measurements is presented and characterized. Test samples are prepared that simulate the arrangement of the wire conductor and multilayer insulation including the healing layer. In initial experiments the capacitance measurements are made using an impedance analyzer. Damage detection circuitry has been developed by NextGen Aeronautics for the purpose of implementing a damage detection and healing algorithm.

3.1 Damage Detection Strategy

The damage detection strategy for the self-healing composite developed in this work is specific to detect damages in a wire insulation with the Surlyn-carbon fiber layer sandwiched between the other insulation layers. Hence the discussion in this chapter and the samples prepared to demonstrate damage detection are application specific. A sample configuration that may be assembled and disassembled without changing capacitance is

necessary so that different amounts of damage can be made to the insulation film. In order to demonstrate and characterize this damage detection technique flat plate type samples are used instead of wire insulation samples for purposes of simplified sample preparation. Electrical access to the carbon fibers in the healing layer is required in order to heal the sample; electrical access to the conductor is required for obvious reasons. Considering that a circuit connection would exist to both the conductor and carbon fibers in the healing layer, it is proposed to detect damage by measuring capacitance between these two 'electrodes'. Capacitive measurements may be used to detect damage in the inner insulation layer(s), located between the conductor and carbon fibers, by using the conductor as one electrode and the carbon fibers in the healing layer as the other electrode. Insulation layers act as capacitors in series, as shown in Fig. 3.1. Damage detection circuitry records a baseline (undamaged) capacitance value and periodically compares a 'current' capacitance value to the baseline. A damage in the polyimide layer, such as a crack, creates a void in the inner insulation layer allows air to flow into the damage and changes the capacitance between the carbon fibers in the healing layer and the conductor. This change in capacitance will serve as a sensing signal in the material. The measured sensing signal will be compared against a baseline to trigger healing. During healing Surlyn would melt, flow, and fill the damage. After healing the circuitry measures and stores a new capacitance baseline.

3.2 Capacitance Measurements

A series of tests were performed to evaluate the amount of capacitance change due to damage in insulation films. If the amount capacitance changes with damage is significant then damage detection via capacitance measurement may be feasible in the wire insulation application. In the first test, two flat plate electrodes measuring 6x11mm were prepared by placing copper tape on acrylic backing plates as shown in Fig. 3.2. Polyimide films with various amounts of damage were placed between the electrodes and the capacitance measured using an Autolab impedance analyzer. Films were damaged by creating a through cut with an x-acto knife. Various levels of damage were achieved by making 2, 4, or 6 cuts. Each cut extended beyond the width dimension of the electrode and had average cut width 100μm. Undamaged films (no cuts) were also measured. The capacitance of a flat

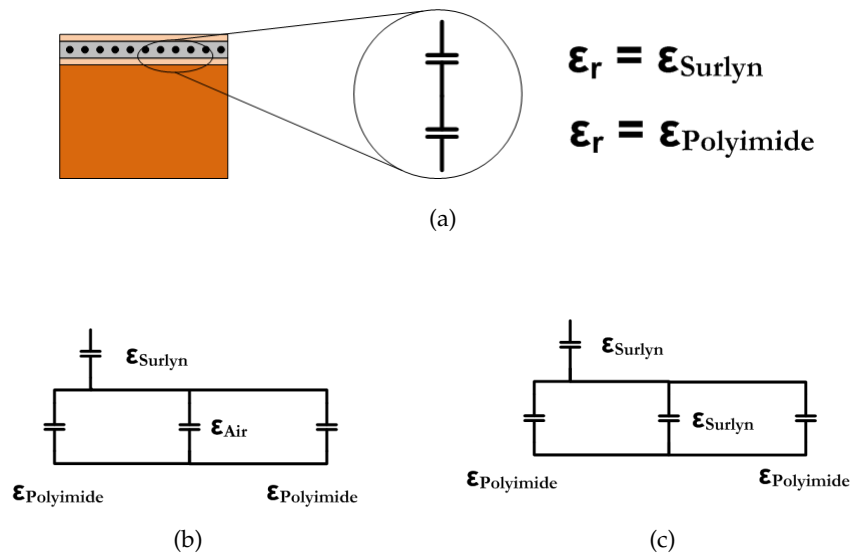

Figure 3.1: Insulation layers act as capacitors in series, using carbon fibers and conductor as electrodes (a). When damaged, capacitance is changed because air flows into the damage (b). During healing Surlyn flows into the damage (c).

plate is given by Eq. (3.1). Damage to the film allows air gaps which change the relative permittivity and area of the dielectric material.

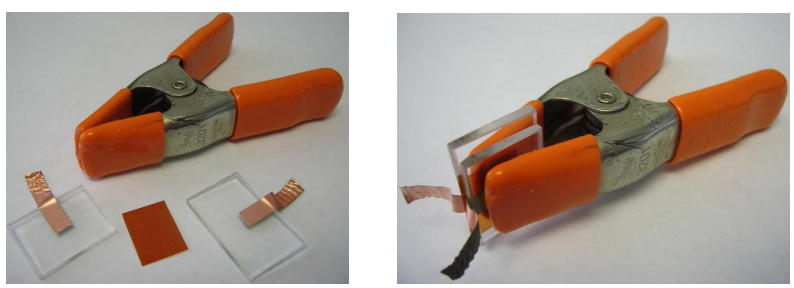

Figure 3.2: Capacitance change with increasing damage in polyimide.

$$C = \epsilon_r \epsilon_o \frac{A}{d} \tag{3.1}$$

where ϵ_r is the relative static permittivity, a material property, ϵ_o is the permittivity of free space, 8.854x10^{-}12 F/m, A is the plate area, and d is the dielectric thickness. As damage increases measured capacitance decreases. When cut area was about 5.5% of total area a 10% decrease in capacitance was observed, demonstrating that damage can be detected

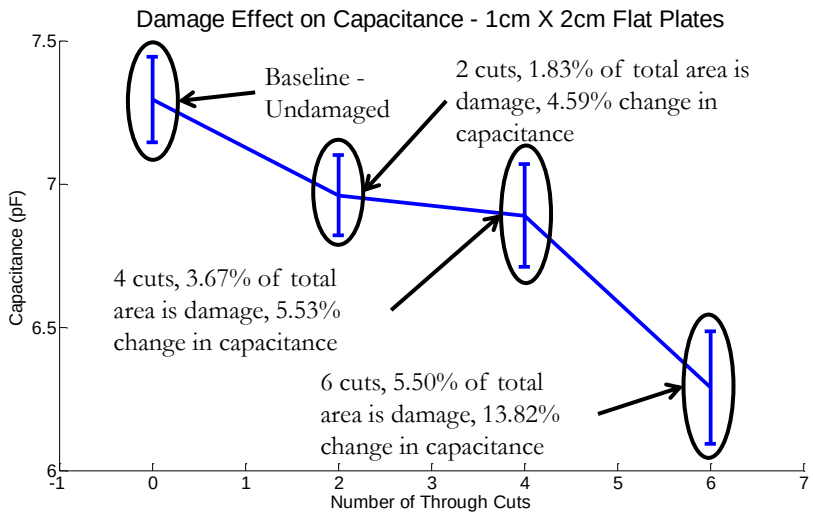

Figure 3.3: Capacitance change with increasing damage in polyimide.

by monitoring change in capacitance. Results are shown in Fig. 3.3.

Following the initial testing, one copper tape electrode was replaced by a carbon fiber (embedded in Surlyn) electrode. In the first testing the capacitor was a polyimide film; in this test the capacitor is formed by Surlyn and polyimide films acting as capacitors in series. Fig. 3.4 shows the electrode configuration. Following the same procedure as before, 13.8% change in capacitance was observed when damage was 5.5% of capacitor area. These results are convincing to use the capacitive damage detection method.

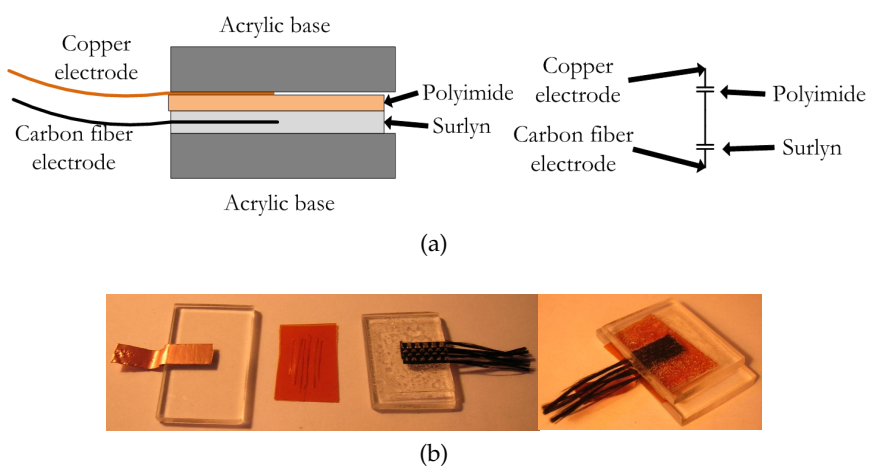

Figure 3.4: Schematic of electrodes (a) and actual electrodes (b).

Capacitive damage detection was successfully demonstrated with the carbon fiber elec-

trode shown in Fig. 3.4, but a modification must be made to that electrode to enable resistive heating. When connecting the carbon fiber in Surlyn electrode in Fig. 3.4 to external circuitry all of the exposed fibers were twisted together making a single connection to the circuitry. To enable resistive heating a carbon fiber in Surlyn electrode is needed that has two connections to the external circuitry so there are positive and negative connections. One way to achieve such an electrode is to arrange carbon fibers as a network of parallel resistors inside Surlyn, with two connections to external circuitry. This electrode is shown in Fig. 3.5.

Figure 3.5: Single connection electrode (left, 98.9% carbon fibers by area) and carbon fibers arranged as a network of parallel resistors inside Surlyn (right, 55.5% carbon fibers by area) with two connections to external circuitry. Both samples measure 13x15mm.

Damage detection capability of the carbon fiber electrodes shown in Fig. 3.5 was compared by measuring capacitance using one carbon fiber electrode and a copper electrode. Polyimide films were damaged as in previous tests. In addition to comparing results with the different carbon fiber electrodes, orientation of damage was tested for the new electrode. Capacitance measurements were recorded for damage parallel to and perpendicular to the network of carbon fiber bundles. Fig. 3.6 shows the results of this testing.

Finally, an experiment was prepared to characterize the capacitance change when there is an additional insulation layer between the healing layer and conductor. This experiment was designed to simulate the TKT wire insulation with healing layer added, so a 2-mil thick PTFE tape insulation layer was first placed on the copper electrode. The polyimide layer is placed on top of the PTFE layer, just under the healing layer. This sample configuration is shown in Fig. 3.7. In this experiment, as in previous experiments, damage was imparted to the insulation in the form of through-cuts in the polyimide film. Progressive

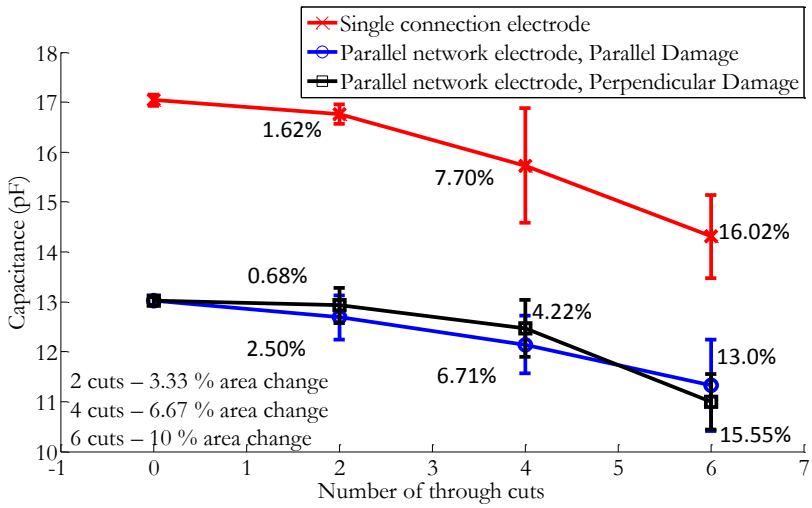

Figure 3.6: Decrease in capacitance with damage trend verified for parallel network carbon fiber electrode. Orientation of damage does not have a significant effect on damage detection ability.

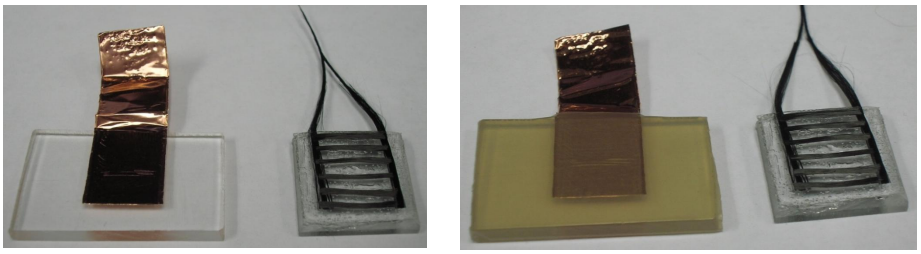

Figure 3.7: Copper and Surlyn/carbon fiber electrodes on acrylic substrates. Electrode area is 13x16mm. Without PTFE (left) and with PTFE (right). Damage layer (polyimide) not shown.

amounts of damage were simulated using 2, 4, and 6 through-cuts.

Baseline (undamaged) capacitance is lower after the PTFE layer is added because this additional layer acts as another capacitor in series with the previous layers. When damage is imparted to the polyimide layer the trend of decreasing capacitance with increasing amount of damage is still evident; capacitance at the highest level of damage (6 through-cuts) is about 6% less than the baseline value. Results of this testing are shown in Fig. 3.8.

3.3 Damage Detection and Healing Circuitry

Damage detection by capacitive measurements is straightforward to integrate with existing electronic systems. In addition to connecting the conductor to electronic circuitry,

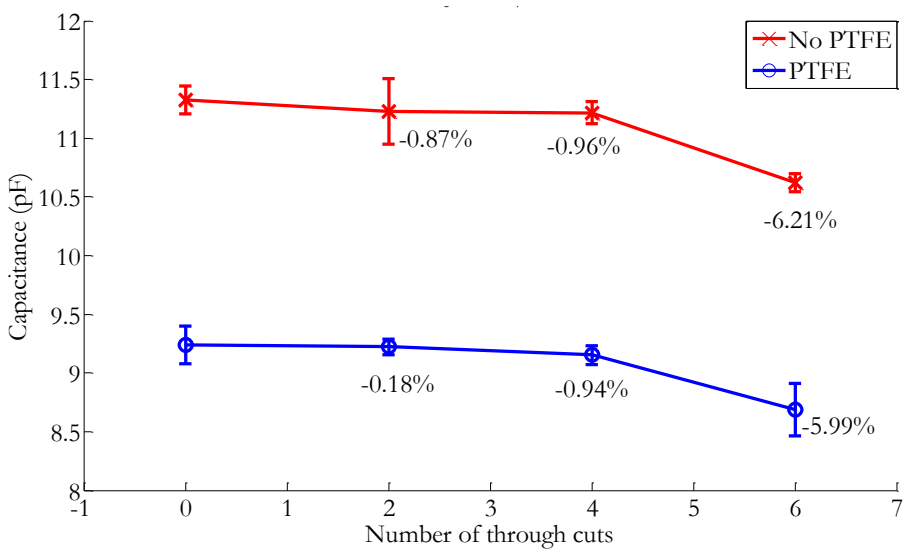

Figure 3.8: Decrease in capacitance with damage trend verified when PTFE layer is added, simulating the current TKT wire insulation with added healing layer.

carbon fibers in the healing layer are also connected in order to enable damage detection and resistive healing. Several methods are well developed for making capacitance measurements, including RC circuit charging response and various AC bridge circuits. Fig. 3.9 shows an algorithm for continuously monitoring the condition of the material. Upon powering on the system baseline measurements are recorded and stored. Measurements are periodically recorded and compared to the baseline measurement. If the difference between the current measurement and the baseline is greater than a predetermined threshold value damage is indicated and healing is triggered. A new baseline is recorded and stored, and the cycle continues. When the wire insulation is prepared with several 'parallel network' zones damage detection may be performed locally to each zone. When damage is detected in any one zone healing is triggered in that zone only; there is no need to heat the entire wire insulation. This technique saves power by heating only the damaged section of the wire insulation.

Electronic circuitry was developed by NextGen Aeronautics to implement this algorithm. The circuit consists of a microcontroller that periodically measures the capacitance of up to 8 channels using an R-C charging scheme. A resistor-capacitor (R-C) circuit with known resistance is charged while tracking the time required. Based on the charge time and known resistance, the value of the capacitance can be calculated. The damage detec-

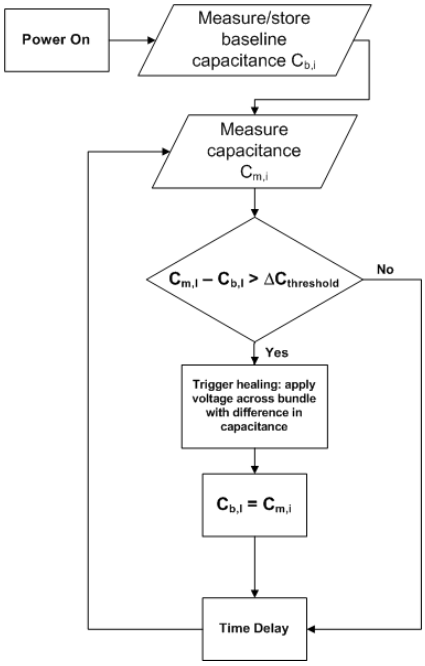

Figure 3.9: Damage detection algorithm.

tion circuit has 8 separate channels capable of storing separate baseline values.

A sample was prepared in order to test the damage detection circuit. This sample was designed to use the parallel network damage detection and healing samples in a geometric arrangement that more closely approximates a wire. This arrangement would demonstrate the damage detection and resistive healing technology but on a larger scale than the actual wire insulation application. A solid copper bar was used as the conductor. Two films were prepared with three damage detection/healing samples arranged side-by-side, for a total of six damage detection/healing zones along the wire. Carbon fiber networks were intentionally prepared with different resistances, by varying the spacing between the electrodes, to demonstrate that the damage detection circuit measures each zone independently. Using this sample the circuit successfully detected damage in the proper zone and triggered healing.

3.4 Chapter Summary

A new damage detection technique using capacitance measurements has been developed. The concept was shown to be capable of detecting damage by detecting a change in mea-

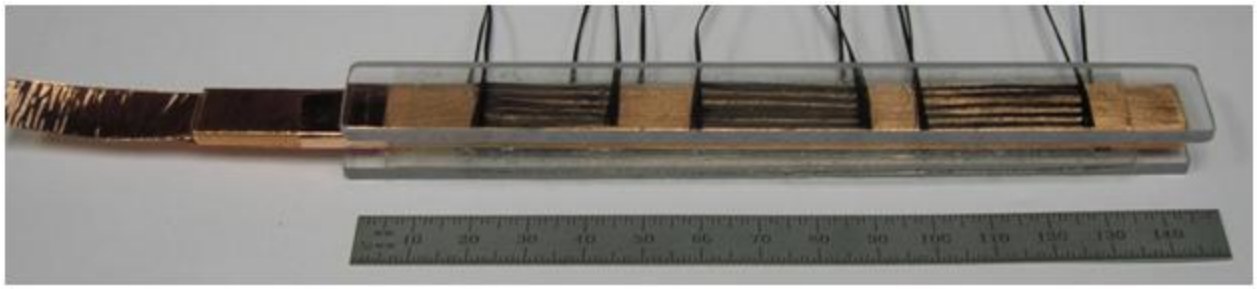

Figure 3.10: Sample prepared for testing the damage detection and healing circuit.

sured capacitance. When damage was 10% of area the change in measured capacitance was 13-15% when using one copper electrode and one carbon fiber electrode. An algorithm has been developed for continuous and autonomous damage monitoring and healing purposes. Electrical circuitry implementing this algorithm has been developed by NextGen Aeronautics and demonstrated successful damage detection and healing capability using parallel network damage detection and healing samples.

CHAPTER 4

MODELING

Healing by resistive heating is demonstrated in the Surlyn/carbon fiber composite in Chapter 2 using samples with uniform distributions of carbon fibers. The healing experiments discussed in Chapter 2 used Surlyn-carbon fiber composite films of arbitrary size. The arrangement of carbon fiber in the polymer matrix was not optimized for healing a surface damage in the sample. Optimizing the arrangement of carbon fibers in Surlyn for a specific application would require manual preparation of a great number of samples followed by characterization tests. To reduce the time and cost in designing the self-healing polymer, a heat transfer model is developed in this chapter that will model the temperature distribution in Surlyn for an applied electric potential across the ends of the carbon fiber. Among the many mathematical modeling techniques the finite element method is well developed based on fundamental principles and can be readily applied to a wide variety of problems. The objective of this modeling effort is to develop an accurate model capable of predicting the temperature distribution to melt the sample at the damage site and initiate healing. The commercial finite element code ABAQUS is used to model resistive heating and subsequent heat transfer to the Surlyn surface where damage is located. Modeling techniques are developed that can be used to reduce development time for future geometrical configurations of the resistive heating/healing material.

4.1 Governing Equations

Healing Surlyn by resistive heating involves several different physical processes. As electrical current flows through the carbon fibers heat is generated in the fibers due to joule heating. This heat is transferred throughout the carbon fiber layer and to the surrounding Surlyn matrix by conduction heat transfer. The thermal energy in the polymer film sus-

pended in air is transferred to the atmospheric gases by convection heat transfer. Heat transfer by conduction in carbon fiber and Surlyn are governed by the general three-dimensional heat conduction equation:

$$\frac{\partial^2 T}{\partial x^2} + \frac{\partial^2 T}{\partial y^2} + \frac{\partial^2 T}{\partial z^2} + \frac{\dot{q}}{k} = \frac{\rho c_p}{k}\frac{\partial T}{\partial t} \tag{4.1}$$

where T is temperature, $\dot{q}$ is the heat flux, k is the thermal conductivity, ρ is the mass density, c_p is the specific heat capacity at constant pressure, and t is time. Resistive heating (Joule heating) is governed by Joule's Law and the thermal energy for an applied current I through th eheating element is given by the formula

$$Q = Pt = I^2 Rt \tag{4.2}$$

where Q is the amount of thermal energy, P is the power, t is time, and R is electrical resistance. Boundary conditions are applied to the general heat conduction equation according to the specific problem. Particularly, the boundary conditions prescribed temperature and convection are applied in this model. The prescribed temperature condition, given by Eq. (4.3), is used to specify the initial temperature of the entire model before the electrical field is applied. Initial temperature is set to room temperature of 21°C. The convection boundary condition, given by Eq. (4.4), is used to model heat transfer out of the composite sample due to natural convection.

$$T_1 = T(x, y, z, t) \tag{4.3}$$

$$(k\frac{\partial T}{\partial x} + h_1 T)_{x=0} = h_1 T \tag{4.4}$$

where h is the convection heat transfer coefficient.

4.2 Modeling Techniques

The objective of the resistive heating model is to predict temperature distribution within the sample for an applied electrical potential across the ends of the carbon fiber heating element. Once this model is developed it can be used by future researchers developing new geometrical configurations of carbon fibers in Surlyn. A finite element model of the

Surlyn/carbon fiber composite, used in the healing experiments discussed in Chapters 2 and 3, is developed. The fabricated sample and its schematic as applied in the model is shown in Fig. 4.1. In the model the carbon fiber heating element is considered to be one continuous thin sheet, instead of individual fiber bundles, for several reasons. Fiber bundle distribution in the fabricated sample is not uniform and adjacent fiber bundles sometimes are in contact with each other. The ideal case of perfectly spaced parallel carbon fiber bundles could be modeled but the resolution of the thermal imaging camera is larger than the distance between bundles. The camera cannot distinguish between adjacent fiber bundles but effectively measures the average temperature of the surface. Electrical current is applied to the carbon fiber and heat is generated due to Joule heating. Heat transfer is modeled by conduction to the surface of Surlyn and by convection out of the top and bottom surfaces of Surlyn.

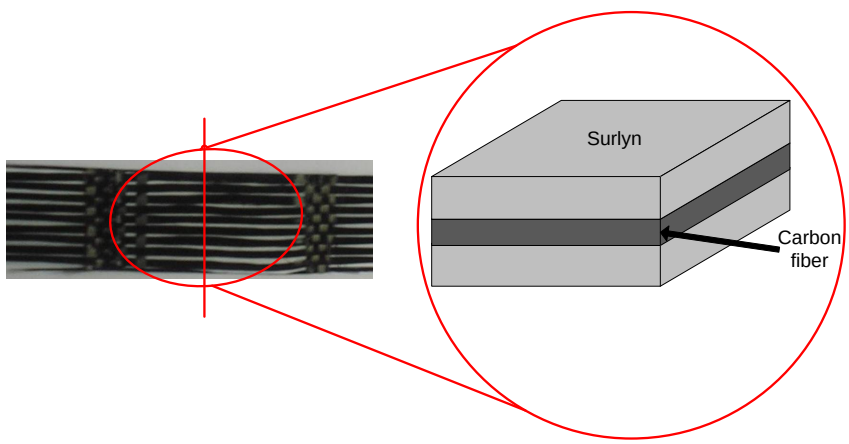

Figure 4.1: Configuration of the Surlyn/carbon fiber resistive heating sample modeled using finite element method.

Measurements on the sample were made using a dial caliper in order to approximate the relevant dimensions. Carbon fiber bundles are approximated as a rectangular film measuring 0.05mm in thickness and 10mm in width. The polymer matrix enclosing the carbon fiber layer is modeled as a rectangular film measuring 0.75mm in thickness and 10mm in width. Length of the carbon fiber heating elements is 20mm.

Carbon fiber bundles were discretized using linear three-dimensional coupled thermal-electrical elements having 8 nodes per element. Surlyn was discretized using linear three dimensional heat transfer elements also having 8 nodes per element. The carbon fiber bun-

dle was meshed with two elements through its thickness, eight elements across its width, and twenty elements along its length. Surlyn was meshed with four elements through its thickness, eight elements across its width, and twenty elements along its length.

Two analysis steps are created. The first step is a steady state heat transfer step and is used for the sole purpose of bringing the entire model up to room temperature of 21°C. A specified temperature boundary condition of 21°C is applied to the whole model the analysis run to steady state conditions. The second step, a transient coupled thermal-electrical analysis step, is created to model joule heating and subsequent heat transfer. In order to facilitate comparisons with resistive heating test data the transient joule heating analysis is run for a time period of 60 seconds. The specified temperature boundary condition of 21°C, applied in the first step, is deactivated for the second step. Electrical current is applied to the end nodes of the carbon fiber.

In order to calculate an appropriate current the resistance of the carbon fiber was estimated using an Autolab PGSTAT 12 and FRA software and was found to be 3.3Ω. Resistive heating experiments conducted on this sample at 2V, 3V, and 5V resulted in current draws of 0.571A, 0.857A, and 1.429A, respectively. In the model it is assumed that all electrical energy is converted to thermal energy by setting the Joule heat fraction equal to one.

Heat is transferred from the carbon fiber heating element to the surrounding Surlyn because the two materials are in thermal contact with one another. In this model thermal contact is assumed to be ideal, that is, there is no resistance to heat flow at the interface of the two materials. A very high thermal contact coefficient for two surfaces in contact corresponds to a very low thermal resistance coefficient.

In the resistive heating/healing test heat is transferred out of the sample by natural convection; the finite element model accounts for this heat transfer. The first step in estimating the convective heat transfer coefficient is to calculate the Rayleigh number according to Eq. (4.5):

$$Ra_L = \frac{g\beta(T_s - T_\infty)L^3}{\nu\alpha} \tag{4.5}$$

Where g is acceleration due to gravity, β is the thermal expansion coefficient, T_s is the surface temperature, T_∞ is the far field temperature, ν is the kinematic viscosity, α is the thermal diffusivity, and L is the length. Thermal images of resistive heating experiments on the same sample geometry, shown in Fig. 2.6, are used to determine surface tempera-

tures. Different convection heat transfer coefficients are calculated for each case because different temperature profiles are observed in the experiments. Surface temperature values at 60 seconds of 41^oC, 71^oC, and 209^oC correspond to experiments conducted at 2V, 3V, and 5V, respectively. Room temperature is 21°C, and the properties of air are listed in Table 4.1.

Table 4.1: Properties of air.

$\beta =$	0.0033	K^{-1}
$\nu =$	$16.2x10^{-6}$	$\frac{\mathrm{m}^2}{\mathrm{s}}$
$\alpha =$	$22.9x10^{-6}$	$\frac{\mathrm{m}^2}{\mathrm{s}}$
$k =$	0.0265	$\frac{\mathrm{W}}{\mathrm{mK}}$

Next, the Nusselt numbers are calculated using the Rayleigh numbers:

$$Nu_L = 0.54 \cdot Ra_L^{\frac{1}{4}} \tag{4.6}$$

Finally, the convective heat transfer coefficients are calculated using the Nusselt numbers:

$$h = \frac{k}{L} \cdot Nu_L \tag{4.7}$$

where k is the thermal conductivity of the air, L is characteristic length, and h is the convective heat transfer coefficient. Table 4.2 lists the results of the Rayleigh numbers, Nusselt numbers, and heat transfer coefficients.

Table 4.2: Heat transfer coefficient for model simulations of different resistive heating experiments.

Experiment	$\mathrm{Ra_L}$	$\mathrm{Nu_L}$	$\mathrm{h}(\frac{\mathrm{W}}{\mathrm{m^2K}})$
2V	13962	5.87	7.78
3V	34905	7.38	9.78
5V	131244	10.28	13.62

The convective heat transfer boundary condition is applied to the outer surfaces of Surlyn as shown in Fig. 4.2. Convective heat transfer out of the sides of the carbon fiber and the end of the sample is ignored due to the small area of those surfaces. Material properties for Surlyn and carbon fiber are listed in Table 4.3. Material properties for carbon

fiber are constant throughout the volume of carbon fiber; paoperties of Surlyn are constant throughout the volume of Surlyn.

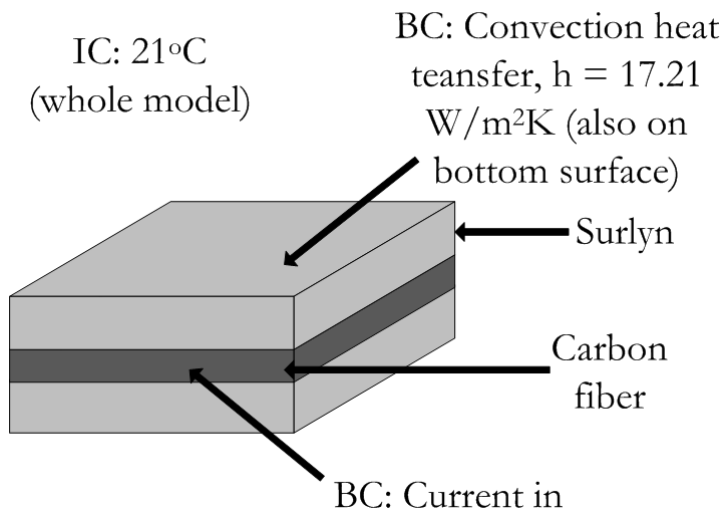

Figure 4.2: Boundary conditions applied to the model.

Table 4.3: Material properties of Surlyn and carbon fiber (CF).

ρ_{Surlyn} =	950	$\frac{\text{kg}}{\text{m}^3}$
k_{Surlyn} =	0.246	$\frac{\text{W}}{\text{mK}}$
$c_{pSurlyn}$ =	2100	$\frac{\text{J}}{\text{kgK}}$
ρ_{CF} =	1800	$\frac{\text{kg}}{\text{m}^3}$
k_{CF} =	15	$\frac{\text{W}}{\text{mK}}$
c_{pCF} =	1000	$\frac{\text{J}}{\text{kgK}}$
$\sigma_{CF,T=21^oC}$ =	68965.5	$\frac{1}{\Omega\text{m}}$

Electrical conductivity varies with temperature, an effect that is included in this model. Given the resistivity at a reference temperature, the resistivity is calculated at other temperatures according to Eq. (4.8). Given the temperature coefficient of resistivity of carbon, α = -0.0005, values of the conductivity of carbon fiber at elevated temperatures are shown in Table 4.4. Linear interpolation is used by the finite element code to evaluate conductivity values between specified temperature-conductivity pairs.

$$R = R_o[1 + \alpha(T - T_o)] \tag{4.8}$$

Table 4.4: Electrical conductivity values as a function of temperature used in the model.

Temperature, ^{o} C	Conductivity, $\frac{1}{\Omega m}$
21	68965
50	67965
100	66241
150	64517
200	62793

4.3 Modeling Results

The objective of developing a finite element model of the resistive heating sample is to develop a means of predicting the temperature distribution within the sample as a function of time. In order to evaluate the accuracy of the model, simulation results are compared to temperature measurements from resistive heating experiments made using a thermal imaging camera. Measurements on resistive heating samples were made on samples with an even distribution of carbon fibers, as shown in Fig. 4.1. Samples were healed at equivalent power levels to resistive heating/healing experiments described in detail in Chapter 2. Temperature data as a function of time was extracted from the finite element model for the center node on the outer surface of Surlyn, representing the average surface temperature of Surlyn.

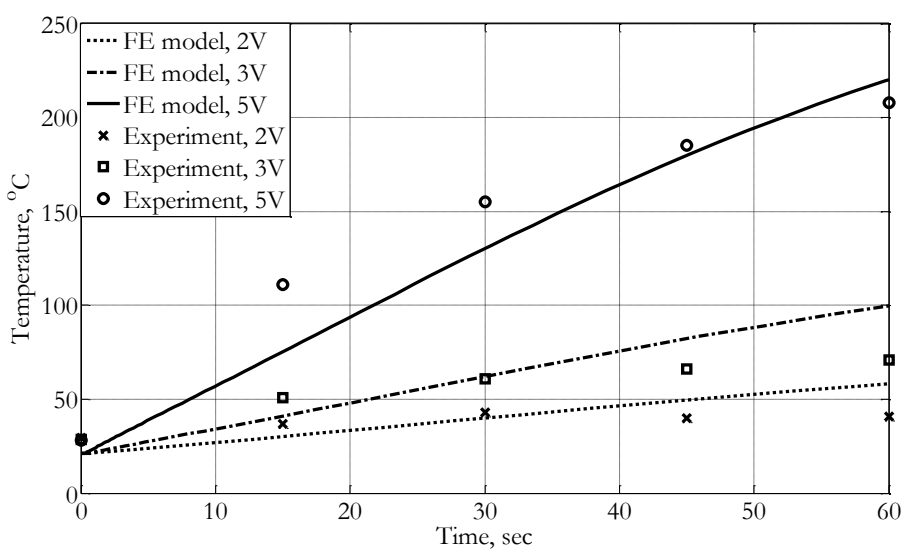

Figure 4.3: Model data compared to temperature measurements made on resistive heating experiments using the thermal imaging camera.

Finite element results predict higher surface temperature and slower temperature rise

than thermal images of resistive heating experiments indicate. There are several potential sources of error leading to inaccuracies in the model. First, the electrical conductivity of carbon fibers used in the resistive heating experiments is difficult to know exactly. Second, not all of the electrical current can be converted to heat in the carbon fibers as is assumed in the model.

4.4 Parallel Network of Carbon Fibers in Surlyn

Thermal images are recorded of resistive heating experiments on parallel network samples. In these samples carbon fiber bundles are arranged as a network of parallel resistors, connected by copper wire leads, embedded in Surlyn. Samples are prepared with carbon fiber heating elements spaced in 5mm increments so that there is sufficient camera resolution to record temperature values between heating elements. A photograph of the sample is shown in Fig. 4.4. Thermal images are recorded using a Fluke Ti25 thermal imaging camera.

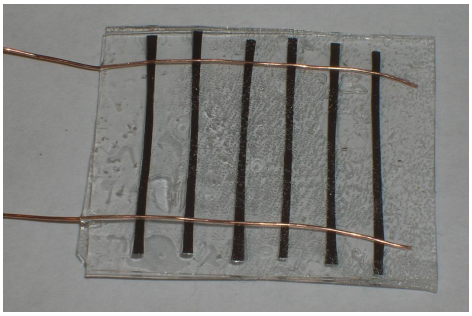

Figure 4.4: Sample used for thermal imaging resistive heating experiments. Spacing of 5mm between heating elements permits temperature measurement between heating elements.

Seven samples are prepared with average resistance 2.5Ω. Resistive heating experiments are carried out at 3V (3.6W), 4V (6.4W), and 5V (10.0W). Thermal images are recorded at 15 second intervals up to the test duration of 60 seconds. Fig. 4.5 shows thermal images of these samples. In all cases the highest temperatures occur at the interface between carbon fiber heating elements and the copper leads. It is believed that high contact resistance between copper and carbon fiber causes the sample to heat more in these areas than in the heating elements.

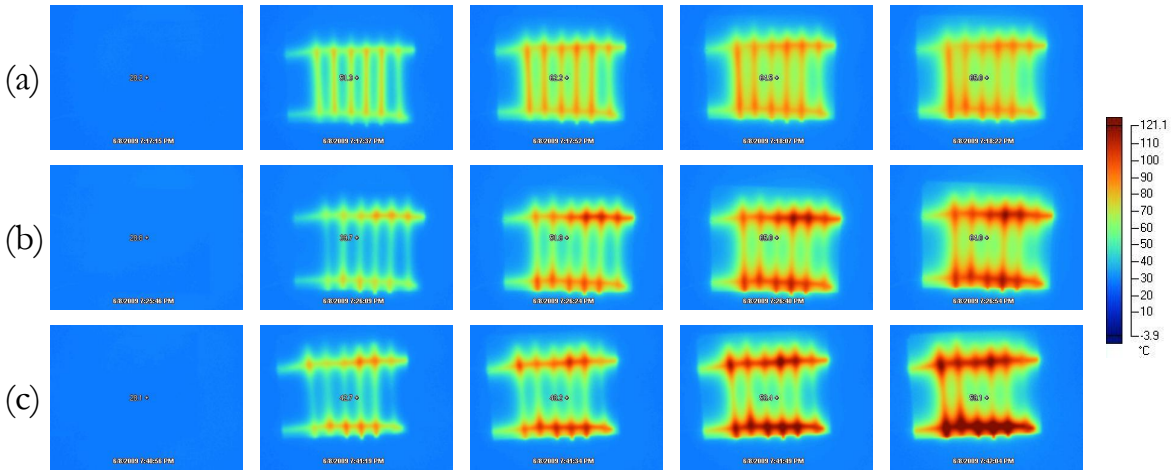

Figure 4.5: Thermal images of resistive heating experiments. The sample is heated at 3.6W (a), 6.4W (b), and 10.0W (c). Test duration increases from t = 0 at left to t = 60sec at right, in 15sec intervals.

Temperature data is extracted and plotted from the thermal images at two locations per image: maximum temperature and average temperature between heating elements. Average temperature between heating elements is determined by measuring the temperature at points midway between two heating elements. Fig. 4.6 shows the average temperature between heating elements as a function of time. Fig. 4.7 shows average temperature at points on the Surlyn surface directly above carbon fiber heating elements as a function of time.

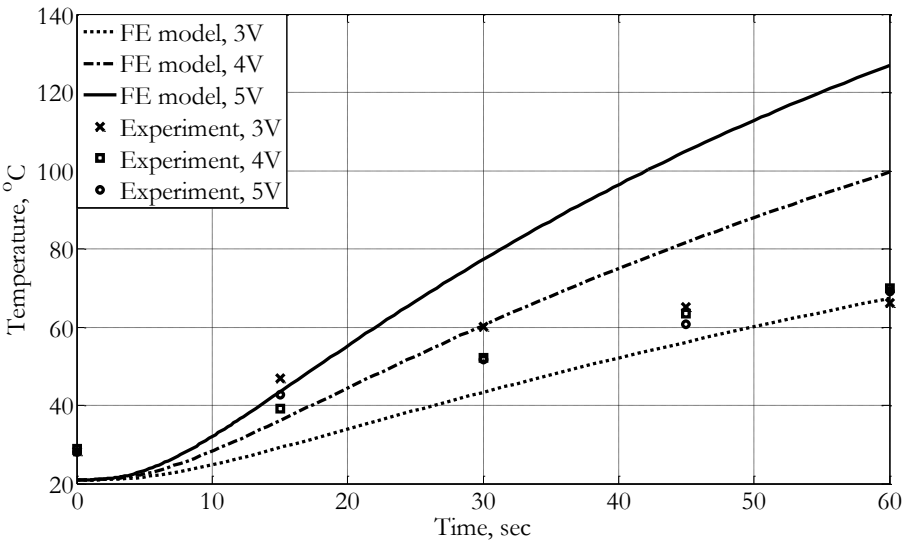

Figure 4.6: Average temperature of points midway between heating elements.

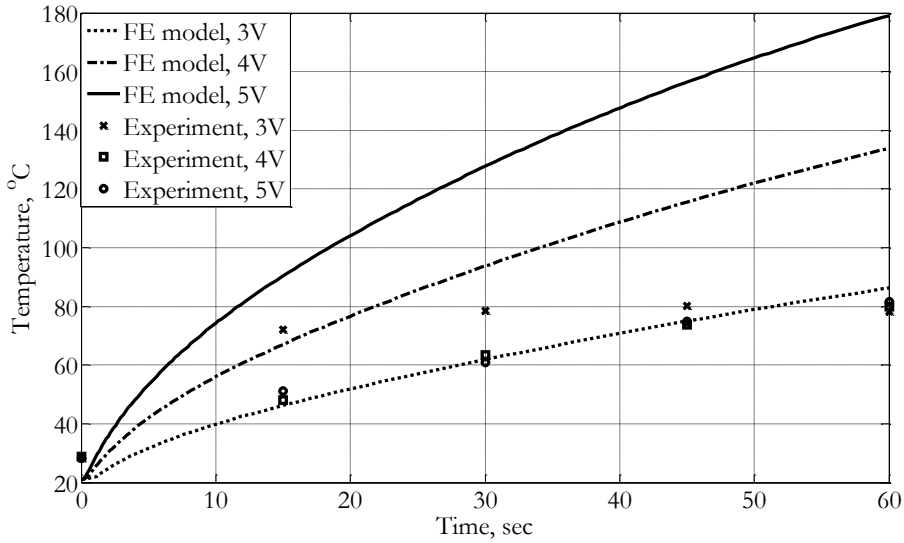

Figure 4.7: Average temperature at points on the Surlyn surface directly above the carbon fiber heating elements.

As shown in the thermal imaging results, Fig. 4.5, high temperature areas are located where carbon fiber heating elements contact the copper wire leads. Higher heat generation in these locations is most likely due contact resistance at the interface of carbon fiber and copper. The finite element model of the parallel network resistive heating sample assumes the ideal case of perfect electrical contact and also assumes that no heat is generated in the copper wire leads because of their relatively low resistance as compared to carbon fiber heating elements. Based on these assumptions, heat generation within the carbon fiber elements was modeled, and not heat generation dur to contact resistance between copper and carbon fiber. Because heat generation occurs primarily due to contact resistance, which is not modeled, the finite element model does not predict accurate temperatures for the parallel network resistive heating sample.

4.5 Chapter Summary

A finite element model of the resistive heating process has been developed to predict temperature distribution within the resistive heating sample. This model consists of a carbon fiber resistive heating element surrounded by Surlyn. Electrical current passes through the carbon fibers and generates heat. Conduction heat transfer through the sample and convective heat transfer out of the sample are modeled. Temperature distribution within the

sample is predicted and compared to experimental measurements with reasonable accuracy for the Surlyn/carbon fiber composite. Modeling techniques used here can be used to predict temperature distributions in future configurations of the resistive heating process, potentially reducing experimental cost and time.

CHAPTER 5

CONCLUSION

5.1 Contributions

The major contribution of this work is the development of a new self-healing composite material with damage detection capability. Development of this material began with a polymer with proven healing capabilities; an electrically conductive network was embedded inside this polymer to enable resistive heating and damage detection. Healing and damage detection capabilities have been demonstrated and characterized. The following list details the steps taken to achieve these results:

- Methods have been developed and used to prepare polymer films and composite samples using those films. Small polymer films were not difficult to produce in a controlled and high-quality way but preparation of larger films and composite samples would benefit from automated mass production methods.

- Composite samples were used to characterize healing capabilities. Samples with uniform distribution were first used to demonstrate resistive heating/healing and characterize power requirements. With power input of 2.5W complete healing was demonstrated in some cases. Other samples, developed to facilitate damage detection, consisting of carbon fibers acting as a network of parallel resistors inside Surlyn. Resistive heating/healing was characterized with these samples but with more varied results due to wider variability in sample resistances.

- Temperature distribution within composite samples during resistive heating experiments was quantified using thermal imaging techniques.

- Healing success was quantified using optical microscopy and tensile testing.

- Damage detection by capacitance measurements was demonstrated and characterized. When damage was 10% of area, measured capacitance was 13-15% lower than baseline (undamaged) capacitance.

- An algorithm for autonomous damage detection and healing has been developed. NextGen Aeronautics has developed and demonstrated a prototype electrical circuit that implements this algorithm using the parallel network samples.

- A finite element model of the resistive heating process used in the composite samples has been developed for the purpose of predicting temperature distribution throughout the sample. This model can be used to assist development of other geometric configurations of this composite material.

5.2 Recommendations for Future Work

In this work a new composite material was developed with demonstrated healing and damage detection capabilities. In order to simplify sample preparation all testing was done using flat plate style samples. The intended application, wire insulation, requires a very different geometrical configuration of this material. A considerable amount of further work with the material and processes developed herein is necessary to demonstrate success in a true wire insulation application.

Improved sample preparation by using automated processes has potential to improve uniformity and ultimate performance of this material. Specifically, automated equipment should be used to position carbon fibers within polymer films and prepare extruded or wrapped wire insulation. After these processes have been developed to prepare wire insulation materials then development efforts can begin to optimize carbon fiber placement within Surlyn in the actual wire insulation geometry instead of an arbitrary flat plate sample. The finite element model of the resistive heating process can be used as a starting point in this development to simulate temperature distribution with different configurations of carbon fibers and evaluate the relative feasibility of different configurations.

Surlyn was chosen for the matrix material due to its proven healing ability other materials may exist that are compatible with the resistive heating process. Initial testing of several ionone materials, developed by the Dr. Long's group in the Chemistry Depart-

ment at Virginia Tech, showed healing potential when heated in an oven. Further development and testing of these or other materials should be conducted in order to select a polymer that best meets the general set of application requirements which includes, but is not limited to, the ability to heal when heated.

While wire insulation was the intended application for this new composite material there are many other potential applications. By changing the arrangement of carbon fibers in Surlyn the properties of the composite can be widely varied. A composite consisting of one or more layers of unidirectional or woven carbon fiber fabric in Surlyn results in a composite material with high tensile stiffness but that maintains flexibility and the ability to change shape when heated, a combination of properties which could prove useful in certain applications.

Bibliography

Abry, J. C., Bochard, S., Chateauminois, A., Salvia, M., and Giraud, G. (1999), "In situ detection of damage in cfrp laminates by electrical resistance measurements," *Composites Science and Technology*, Vol. 59, No. 6, pp. 925 – 935.

Angelidis, N. and Irving, P. (2007), "Detection of impact damage in cfrp laminates by means of electrical potential techniques," *Composites Science and Technology*, Vol. 67, No. 3-4, pp. 594 – 604.

Aragn, A. M., Wayer, J. K., Geubelle, P. H., Goldberg, D. E., and White, S. R. (2008), "Design of microvascular flow networks using multi-objective genetic algorithms," *Computer Methods in Applied Mechanics and Engineering*, Vol. 197, No. 49-50, pp. 4399 – 4410.

Balazs, A. C. (2007), "Modeling self-healing materials," *Materials Today*, Vol. 10, No. 9, pp. 18 – 23.

Barbero, E. J., Greco, F., and Lonetti, P. (2005), "Continuum Damage-healing Mechanics with Application to Self-healing Composites," *International Journal of Damage Mechanics*, Vol. 14, No. 1, pp. 51–81.

Bejan, A., Lorente, S., and Wang, K.-M. (2006), "Networks of channels for self-healing composite materials," *Journal of Applied Physics*, Vol. 100, No. 3, 033528.

Blaiszik, B., Sottos, N., and White, S. (2008), "Nanocapsules for self-healing materials," *Composites Science and Technology*, Vol. 68, No. 3-4, pp. 978 – 986.

Brown, E., White, S., and Sottos, N. (2005), "Retardation and repair of fatigue cracks in a microcapsule toughened epoxy composite - part i: Manual infiltration," *Composites Science and Technology*, Vol. 65, No. 15-16, pp. 2466 – 2473.

Brown, S. and White (2002), "Fracture testing of a self-healing polymer composite," *Experimental Mechanics*, Vol. 42, No. 4, pp. 372 – 379.

Burton, D., Gao, X., and Brinson, L. (2006), "Finite element simulation of a self-healing shape memory alloy composite," *Mechanics of Materials*, Vol. 38, No. 5-6, pp. 525 – 537.

Carlson, J. A., English, J. M., and Coe, D. J. (2006), "A flexible, self-healing sensor skin," *Smart Materials and Structures*, Vol. 15, No. 5, pp. N129–N135.

Chen, X., Dam, M. A., Ono, K., Mal, A., Shen, H., Nutt, S. R., Sheran, K., and Wudl, F. (2002), "A Thermally Re-mendable Cross-Linked Polymeric Material," *Science*, Vol. 295, No. 5560, pp. 1698–1702.

Davila, A., Garnica, G., Lopez, J., and Carrion, F. (2009), "Fatigue damage detection using a speckle-contrast technique," *Optics and Lasers in Engineering*, Vol. 47, No. 3-4, pp. 398 – 402.

Dickinson, L. and Fletcher, N. (2009), "Acoustic detection of invisible damage in aircraft composite panels," *Applied Acoustics*, Vol. 70, No. 1, pp. 110 – 119.

Doebling, S. W., Farrar, C. R., and Prime, M. B. (1998), "Summary review of vibration-based damage identification methods," *Shock and Vibration Digest*, Vol. 30, No. 2, pp. 91 – 105.

Doebling, S. W., Farrar, C. R., Prime, M. B., and Shevitz, D. W. (1996), "Damage identification and health monitoring of structural and mechanical systems from changes in their vibration characteristics: A literature review." , pp. 133p –.

Dry, C. M. and Sottos, N. R. (1993), "Passive smart self-repair in polymer matrix composite materials," Vol. 1916, pp. 438–444.

Gupta, S., Singh, D. S., and Ray, A. (2008), "Statistical pattern analysis of ultrasonic signals for fatigue damage detection in mechanical structures," *NDTE International*, Vol. 41, No. 7, pp. 491 – 500.

Jones, M. S., Rule and White (2007), "Life extension of self-healing polymers with rapidly growing fatigue cracks," *J R Soc Interface*, Vol. 4, No. 13, pp. 395 – 403.

Kalista (2003), *Self-Healing of Thermoplastic Poly(Ethylene-co-Methacrylic Acid) Copolymers Following Projectile Puncture*, Master's thesis, Virginia Polytechnic Institute and State University.

Kalista and Ward (2007), "Thermal characteristics of the self-healing response in poly(ethylene-co-methacrylic acid) copolymers." *J R Soc Interface*, Vol. 4, No. 13, pp. 405 – 411.

Keller, S., White (2007), "A self-healing poly(dimethyl siloxane) elastomer," *Advanced Functional Materials*, Vol. 17, pp. 2399 – 2404.

Kessler, M. R., Sottos, N. R., and White, S. R. (2003), "Self-healing structural composite materials," *Composites Part A: Applied Science and Manufacturing*, Vol. 34, No. 8, pp. 743 – 753.

Kwok, N. and Hahn, H. T. (2007), "Resistance Heating for Self-healing Composites," *Journal of Composite Materials*, Vol. 41, No. 13, pp. 1635–1654.

Lee, J. Y., Buxton, G. A., and Balazs, A. C. (2004), "Using nanoparticles to create self-healing composites," *The Journal of Chemical Physics*, Vol. 121, No. 11, pp. 5531–5540.

Maiti, S., Shankar, C., Geubelle, P. H., and Kieffer, J. (2006), "Continuum and molecular-level modeling of fatigue crack retardation in self-healing polymers," *Journal of Engineering Materials and Technology*, Vol. 128, No. 4, pp. 595–602.

Martin, L. A. (2004), *Developing a Self-Powered, Wireless Damage Detection System for Structural Health Monitoring Applications*, Master's thesis, Virginia Polytechnic Institute and State University.

Montalvao, M. and Ribeiro (2006), "A review of vibration based structural health monitoring with special emphasis on composite materials," *The Shock and Vibration Digest*, Vol. 38, No. 4, pp. 295 – 324.

N. Sottos, I. B., S. White (2007), "Introduction: self-healing polymers and composites," *J R Soc Interface*, Vol. 4, No. 13, pp. 347 – 348.

Owen, C. C. (2006), *Magnetic Induction for In-situ Healing of Polymeric Material*, Master's thesis, Virginia Polytechnic Institute and State University.

Park, J. S., Takahashi, K., Guo, Z., Wang, Y., Bolanos, E., Hamann-Schaffner, C., Murphy, E., Wudl, F., and Hahn, H. T. (2008), "Towards Development of a Self-Healing Composite using a Mendable Polymer and Resistive Heating," *Journal of Composite Materials*, Vol. 42, No. 26, pp. 2869–2881.

Park, S., Yun, C.-B., Roh, Y., and Lee, J.-J. (2006), "Pzt-based active damage detection techniques for steel bridge components," *Smart Materials and Structures*, Vol. 15, No. 4, pp. 957–966.

Privman, V., Dementsov, A., and Sokolov, I. (2007), "Modeling of self-healing polymer composites reinforced with nanoporous glass fibers," *Journal of Computational and Theoretical Nanoscience*, Vol. 4, p. 190.

R. S Trask, G. J. W. and Bond, I. P. (2007), "Bioinspired self-healing of advanced composite structures using hollow glass fibres," *J R Soc Interface*, Vol. 4, No. 13, pp. 363 – 371.

Rule, J. D., Sottos, N. R., and White, S. R. (2007), "Effect of microcapsule size on the performance of self-healing polymers," *Polymer*, Vol. 48, No. 12, pp. 3520 – 3529.

Salawu, O. S. (1997), "Detection of structural damage through changes in frequency: a review," *Engineering Structures*, Vol. 19, No. 9, pp. 718 – 723.

Tiefenbach, A., Wagner, S., Oberacker, R., and Hoffmann, B. (2000), "The use of impedance spectroscopy in damage detection in tetragonal zirconia polycrystals (tzp)," *Ceramics International*, Vol. 26, No. 7, pp. 745 – 751.

Toohey, K. S., Sottos, N. R., Lewis, J. A., Moore, J. S., and White, S. R. (2007), "Self-healing materials with microvascular networks," *Nat Mater*, Vol. 6, No. 8, pp. 581 – 585.

Trask, R. S. and Bond, I. P. (2006), "Biomimetic self-healing of advanced composite structures using hollow glass fibres," *Smart Materials and Structures*, Vol. 15, No. 3, pp. 704–710.

Trask, W. and Bond (2007), "Self-healing polymer composites: mimicking nature to enhance performance," *Bioinspiration & Biomimetics*, Vol. 2, No. 1, pp. P1–P9.

Varley, R. J. and van der Zwaag, S. (2008a), "Development of a quasi-static test method

to investigate the origin of self-healing in ionomers under ballistic conditions," *Polymer Testing*, Vol. 27, No. 1, pp. 11 – 19.

Varley, R. J. and van der Zwaag, S. (2008b), "Towards an understanding of thermally activated self-healing of an ionomer system during ballistic penetration," *Acta Materialia*, Vol. 56, No. 19, pp. 5737 – 5750.

Wang, X. (2007), *Application of Single-part Adhesives as Healing Agent in Self-Healing Composites*, Master's thesis, The University of New South Wales.

Wen, S. and Chung, D. (2007), "Electrical-resistance-based damage self-sensing in carbon fiber reinforced cement," *Carbon*, Vol. 45, No. 4, pp. 710 – 716.

White, S. R., Sottos, N. R., Geubelle, P. H., Moore, J. S., Kessler, M. R., Sriram, S. R., Brown, E. N., and Viswanathan, S. (2001), "Autonomic healing of polymer composites," *Nature*, Vol. 409, No. 6822, pp. 794 – 797.

Williams, B., Boydston (2007), "towards electrically conductive, self-healing materials," *J R Soc Interface*, Vol. 4, No. 13, pp. 359 – 362.

Williams, G., Trask, R., and Bond, I. (2007a), "A self-healing carbon fibre reinforced polymer for aerospace applications," *Composites Part A: Applied Science and Manufacturing*, Vol. 38, No. 6, pp. 1525 – 1532.

Williams, H. R., Trask, R. S., and Bond, I. P. (2007b), "Self-healing composite sandwich structures," *Smart Materials and Structures*, Vol. 16, No. 4, pp. 1198–1207.

Williams, K. W., Trask and Bond (2007), "Biomimetic reliability strategies for self-healing vascular networks in engineering materials," *J R Soc Interface*, Vol. 5, No. 24, pp. 735 – 747.

Williams, W., Trask and Bond (2008), "Minimum mass vascular networks in multifunctional materials," *J R Soc Interface*, Vol. 5, No. 18, pp. 55 – 65.

Wu, D. Y., Meure, S., and Solomon, D. (2008), "Self-healing polymeric materials: A review of recent developments," *Progress in Polymer Science*, Vol. 33, No. 5, pp. 479 – 522.

Yin, T., Rong, M. Z., Zhang, M. Q., and Yang, G. C. (2007), "Self-healing epoxy composites - : Preparation and effect of the healant consisting of microencapsulated epoxy and latent curing agent," *Composites Science and Technology*, Vol. 67, pp. 201 – 212.

Zhou, G. and Sim, L. M. (2002), "Damage detection and assessment in fibre-reinforced composite structures with embedded fibre optic sensors-review," *Smart Materials and Structures*, Vol. 11, No. 6, pp. 925–939.